The effect of horizontal resolution on Indian monsoon depressions in the Met Office NWP model

RMetS
Royal Meteorological Society

The effect of horizontal resolution on Indian monsoon depressions in the Met Office NWP model

Kieran M.R. Hunt[a]* and Andrew G. Turner[a,b]
[a]*Department of Meteorology, University of Reading, UK*
[b]*NCAS-Climate, University of Reading, UK*

*Correspondence to: K. M. R. Hunt, Department of Meteorology, University of Reading, Earley Gate, PO Box 243, Reading, RG6 6BB, UK. E-mail: k.m.r.hunt@reading.ac.uk

Monsoon depressions are synoptic-scale features that are responsible for a significant fraction of the rain over northern India during the summer monsoon season, and therefore it is important to quantify their structure and behaviour in numerical weather prediction (NWP) models. It is known that increasing model resolution is strongly correlated with improved forecasts in the short term and global circulation in the longer term, as well as better representation of tropical cyclones; here, we explore the sensitivity of depressions to changes in resolution using the Met Office Unified Model. Seven NWP case-studies of depressions from 2013 to 2015 were run at eight resolutions corresponding to equatorial grid spacing of between 16 and 208 km, and compared with data for the same events from Tropical Rainfall Measuring Mission (TRMM) and ERA-Interim reanalysis. We found that, at the low-resolution end of the spectrum, increases in resolution led to improvements in the composite structure, but with diminishing returns; that is to say, the improvements in forecast track and structure become smaller. The model also persistently overestimated the depression intensity, in particular the wind speed and the warm core aloft–with the source appearing to originate in the mid-troposphere. The sensitivity of the diurnal cycle to resolution was also explored: the stratiform component was found to be very well represented by the model, whereas the convective component was described quite poorly. Improvement in most components of structure with increasing model resolution were marginal beyond N320 (63 km) and N512 (39 km) for dynamic and thermodynamic fields respectively.

Key Words: monsoon; depression; NWP; model resolution; TRMM; ERA-Interim

Received 15 November 2016; Revised 14 February 2017; Accepted 2 March 2017; Published online in Wiley Online Library 19 May 2017

1. Introduction

Indian monsoon depressions (MDs) are synoptic-scale systems that typically spin up over the Bay of Bengal before propagating northwestward over the Indian subcontinent and terminating over northwest India or Pakistan (Godbole, 1977; Hurley and Boos, 2015; Hunt *et al.*, 2016a). Despite the otherwise highly favourable conditions, strong vertical wind shear during the Indian monsoon prevents depressions from further deepening into tropical cyclones; however, they still bring significant and occasionally devastating precipitation to agrarian north India, and are responsible for modulating the majority of the seasonal (June–September) rainfall there (Mooley, 1973). They have an average duration of around 5 days, and generally occur between two and four times per season. Despite their clear importance, little has been done to evaluate their representation in models, or their sensitivity to changes therein.

Numerical model resolution has consistently been shown to play a critical role in both deterministic (Mass *et al.*, 2002) and ensemble (Buizza *et al.*, 1998) forecasts; at all spatial scales: e.g. mesoscale (Bryan and Morrison, 2012), synoptic (Hill and Lackmann, 2009; Murakami and Sugi, 2010) and global (Roeckner *et al.*, 2006); all time-scales: e.g. climate (Roeckner *et al.*, 2006; Johnson *et al.*, 2016) and weather (Mass *et al.*, 2002); all locations: e.g. the Asian monsoon (Sperber *et al.*, 1994; Johnson *et al.*, 2016) and polar regions (Boville, 1991); and across a number of processes (Pope and Stratton, 2002), particularly for those involving precipitation (Giorgi and Marinucci, 1996). While there has been much work undertaken to determine the sensitivity of tropical cyclone structure and intensity to model resolution (e.g. Gentry and Lackmann, 2010; Strachan *et al.*, 2013), no such study has been carried out for MDs. These studies leave little doubt that increasing horizontal resolution in a deterministic model gives improved forecasts, that is to say that, for a given lead time, the structure of meteorological fields becomes closer to those observed during analysis. However these increases in resolution come at at a significant computational cost, and it is important to determine whether similar improvements could be gained more cheaply by focussing on improvement of model parametrizations.

Table 1. A summary of the seven monsoon depressions used in this study.

Start time (UTC) and date	Duration (h)	Mean speed ($m\,s^{-1}$)	Heading (°)
0000 30 Jul 2013	40	6.1	281
0000 20 Aug 2013	54	4.9	278
0000 21 Jul 2014	48	5.8	273
1200 03 Aug 2014	71	4.8	294
0000 20 Jun 2015	40	2.9	334
0000 10 Jul 2015	51	6.8	309
0000 16 Sep 2015	60	6.4	280

Data are computed directly from the high-resolution IMD eAtlas tracks. Duration is defined as the total (contiguous) time for which the IMD classified the disturbance as a depression.

In this study, we propose to disentangle this problem using the numerical weather prediction (NWP) framework of the Met Office Unified Model (MetUM). This can be run globally at a large range of horizontal resolutions, allowing us to probe how well MDs are represented overall and at what resolutions important processes are well illustrated.

We start with a discussion on the experimental set-up of the MetUM, along with the tracking algorithm and other data sources used in section 2. We then examine how the MD propagation and duration is affected by resolution in section 3, before extending this intercomparison to the monsoon trough itself in section 4. We then examine the composite MD structure in a selection of fields in section 5, discussing horizontal (section 5.2) and vertical structure (section 5.1) and presenting a detailed analysis of the diurnal cycle of precipitation (section 5.4).

2. The Met Office Unified Model and experimental set-up

Here, we outline the experimental set-up and the data used. We open with a discussion of the case-study selection before looking at the MetUM and how we have set it up to work at a range of horizontal resolutions. We then discuss the method used to track MDs in our data, and an algorithm developed to allow fair comparison of fields at different resolutions. We conclude this section with a discussion on external data sources.

2.1. Case-study selection

Seven MDs were selected from the IMD eAtlas (http://www.rmcchennaieatlas.tn.nic.in; accessed 29 March 2017) subject to the following criteria: firstly, the genesis point should be in or near the Bay of Bengal so that the governing circulation and orography is inter-comparable; secondly, they should be recent, to ensure the analysis from which the forecast is initiated has high resolution and is of good quality; and thirdly, that the MD featured notable spatial propagation – some spin up near the coast and simply do not have coherent propagation, despite lasting for several days or longer, and these were not selected. A summary of these seven MDs is given in Table 1; they represent a good spread of mean headings (despite the typically low variance in this field (Hunt and Parker, 2016)), durations, propagation speeds, and timing with the monsoon season. This is a reasonable sample size, larger than that of Godbole (1977) or Stano *et al.* (2002), comparable with Sarker and Choudhary (1988), but smaller than the climatological studies of Hurley and Boos (2015) and Hunt *et al.* (2016a). The India Meteorological Department uses a subjective method with synoptic surface charts to track and classify incident monsoon disturbances (hereafter referred to as IMD tracks) which contrasts with our objective method; we have independently tracked these disturbances (hereafter referred to as ERA-I tracks) subject to the criteria discussed earlier in this section using ERA-Interim data (Dee *et al.*, 2011). Figure 1 shows a comparison of these track pairs. Note that the MDs we tracked objectively from reanalysis data tend to have longer durations than the official MDs declared by the IMD due to our weaker wind criterion ($<8.5\,m\,s^{-1}$ at 850 hPa rather than at the surface).

2.2. Overview of the Unified Model

The version of the Met Office Unified Model (MetUM) used for this study runs version 6 of the Global Atmosphere (GA6) and JULES Global Land (GL6) configuration (Walters *et al.*, 2016). The current dynamical core of the MetUM (ENDGame; Wood *et al.*, 2014) solves the non-hydrostatic, fully compressible, deep-atmosphere equations of motion using a semi-implicit semi-Lagrangian scheme on a regular latitude/longitude grid, with an explicit diffusion scheme. Regardless of horizontal resolution, it was run with 85 vertical levels; this corresponds to a resolution of about 100 m in the lower troposphere, decreasing to more than 5 km in the thermosphere with a lid at 85 km (0.004 hPa). A number of parametrizations are also implemented, including:

2.2.1. Convection

The scheme proposed by Gregory and Rowntree (1990) forms the basis of the convective parametrization used in the MetUM. This is extended to include phenomena including downdraughts (Gregory and Allen, 1991) and depth-specific convective momentum transport – shallow (Grant and Brown, 1999; Grant, 2001), mid-level (Gregory *et al.*, 1997), deep (Stratton *et al.*, 2009)). CAPE closure is used for mid-level and deep convection and, with some exceptions for stability, is fixed at 1 h (Fritsch and Chappell, 1980).

2.2.2. Sub-grid orography

Effects from subgrid-scale orography can accumulate to become important on the larger scale; in our study, the most relevant example of this is the potential for mechanical convection to be forced by the unresolved features of the Western Ghats and Himalayan foothills. In the MetUM, effects on this intermediate scale (which also include orographic drag) are handled by a scheme based on Lott and Miller (1997), whereas finer-scale interactions involving stress and torque from roughness friction are estimated by a scheme based on Wood and Mason (1993).

2.2.3. Turbulent mixing

A scheme based on Lock *et al.* (2000) with extensions from Lock (2001) and Brown *et al.* (2008) is used to parametrize turbulence in the MetUM. This scheme also largely governs motion in the atmospheric boundary layer (for which it was originally intended), upholding adiabatic conservation laws with a first-order turbulence closure.

2.2.4. Precipitation and cloud

Local convective precipitation is handled directly by the convection scheme (see above). However, much of the rainfall associated with monsoon depressions is stratiform in nature due to the large-scale moisture convergence they induce in the lower troposphere (Hunt *et al.*, 2016b). This is handled by a scheme based on Wilson and Ballard (1999), with specific precipitation extensions based on discussions in Tripoli and Cotton (1980), Abel and Shipway (2007), Abel *et al.* (2010), and Abel and Boutle (2012). Cloud fraction and condensate are computed using a prognostic scheme (Wilson *et al.*, 2008).

In this experiment, we keep fairly close to the operational use of the model by the Met Office. That is to say, it is run globally and with forced, persisted sea-surface temperatures (SSTs) in atmosphere-only mode, although we perform no data assimilation. The model physics and parametrizations do not

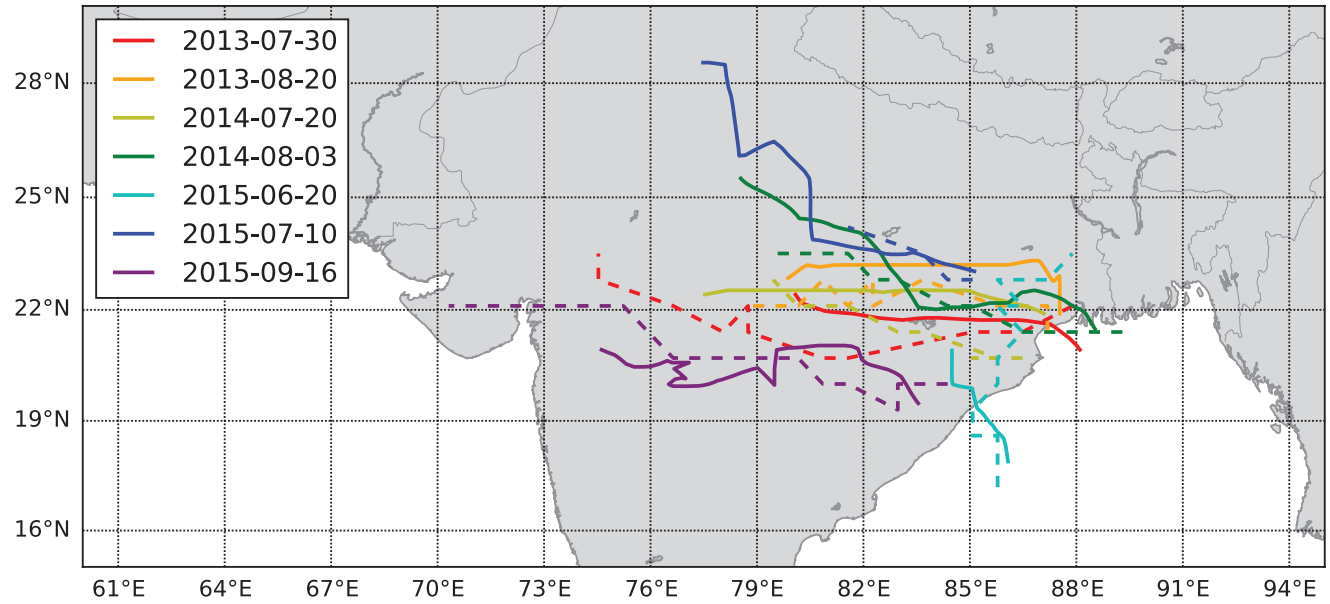

Figure 1. Comparison of official IMD tracks (solid) with those tracked objectively from ERA-Interim (dashed). The average length of the latter is greater due to the relaxed MD wind criterion used in this study. Depression start dates are given in Table 1.

Table 2. A summary of the eight horizontal resolutions used in this study, with dimensions of the global grid, and zonal resolution at the Equator.

Name	Grid points ($n_x \times n_y$)	Resolution (km)
N96	192 × 144	208
N216	432 × 324	93
N320	640 × 480	63
N512	1024 × 768	39
N640	1280 × 960	31
N768	1526 × 1152	26
N1024	2048 × 1536	20
N1280	2560 × 1920	16

n_x and n_y refer to the number of longitudes and latitudes respectively used to construct the grid.

change as a function of resolution; the model time step of 15 min is stable at all resolutions.

2.3. *The spectrum of resolutions*

For this study, the NWP model was run over eight resolutions, ranging from that currently used for the Met Office Hadley Centre low-resolution climate model, increasing to the current NWP forecasting model resolution of N768, through to two higher resolutions expected to be operational in the near future (N1024 and N1280). A summary of these resolutions including the number of grid points they use and the approximate zonal grid point spacing at the Equator is given in Table 2. For each of the seven case-studies, the NWP model was run at all eight resolutions, with a fixed 70 vertical levels; the initiation date for each forecast was selected as 0000 UTC on the day before the IMD officially declared the depression.

2.4. *Description of the tracking algorithm*

We use the fixed-domain objective feature-based tracking algorithm described by Hunt *et al.* (2016a) and improved by Hunt *et al.* (2016b), which filters vortical events subject to the criteria discussed in the Introduction (at least two closed even* hPa isobars; surface wind speeds in excess of 8.5 m s^{-1}). Since ancillary surface roughness lengths vary significantly with model resolution and have a strong effect on surface winds, we adopt a slight scale-invariant adaptation: we use 850 hPa wind as the primary tracking criterion. If resolution were not variable, we would use the IMD criteria recently mentioned, i.e. closed surface isobars over land and surface wind speed over the ocean. This has the clear caveat of being more sensitive to weaker disturbances as MD winds tend to reach a maximum just above the boundary layer (Hunt *et al.*, 2016a), and we shall subsequently accept that some parts of the resulting MD tracks would technically be classified as monsoon lows.

2.5. *Adaptive downsampling*

During the course of this study, we will be exploring data represented at resolutions spanning more than an order of magnitude. This presents a problem with comparative analysis, particularly for fields with a high spatial frequency, such as vorticity. Conventionally, increasing or slightly decreasing resolution is achieved by some optimal-order bivariate interpolation; however this can–and will, beyond a certain point–cause significant aliasing problems, even at high interpolation orders. This means that the data become misrepresented, particularly when looking for extreme values (e.g. in determining the maximum intensity a system achieves). To circumvent this, we must consider what it means to represent data at lower resolutions–it is, essentially, *zooming out*; thus we should expect to be able to traverse to a low-resolution grid, L (size: $L_l \times L_w$), from a higher-resolution grid, H ($aL_l \times bL_w : a, b \in \mathbb{Z}$), via a block-mean reduction of the form:

$$L_{ij} = \frac{1}{ab} \sum_{k=ai}^{a(i+1)} \sum_{l=bj}^{b(j+1)} H_{km} \,. \tag{1}$$

It is reasonable to assume that, in a real-world application, a and b will not necessarily be integers; in this case it is safe to perform the above using their floors and then trivial to apply a suitable (in our case, biquintic–i.e. fifth order polynomial–splines in each dimension) interpolater to the lower-resolution data to adjust it to the required resolution. An example of this procedure is shown pictorially in Figure 2 for an 8 × 8 to 3 × 3 conversion.

2.6. *Data sources*

This study makes some use of external datasets. Firstly, the ERA-Interim reanalysis product (Dee *et al.*, 2011) from the European

*i.e. . . . , 998, 1000, 1002, . . .

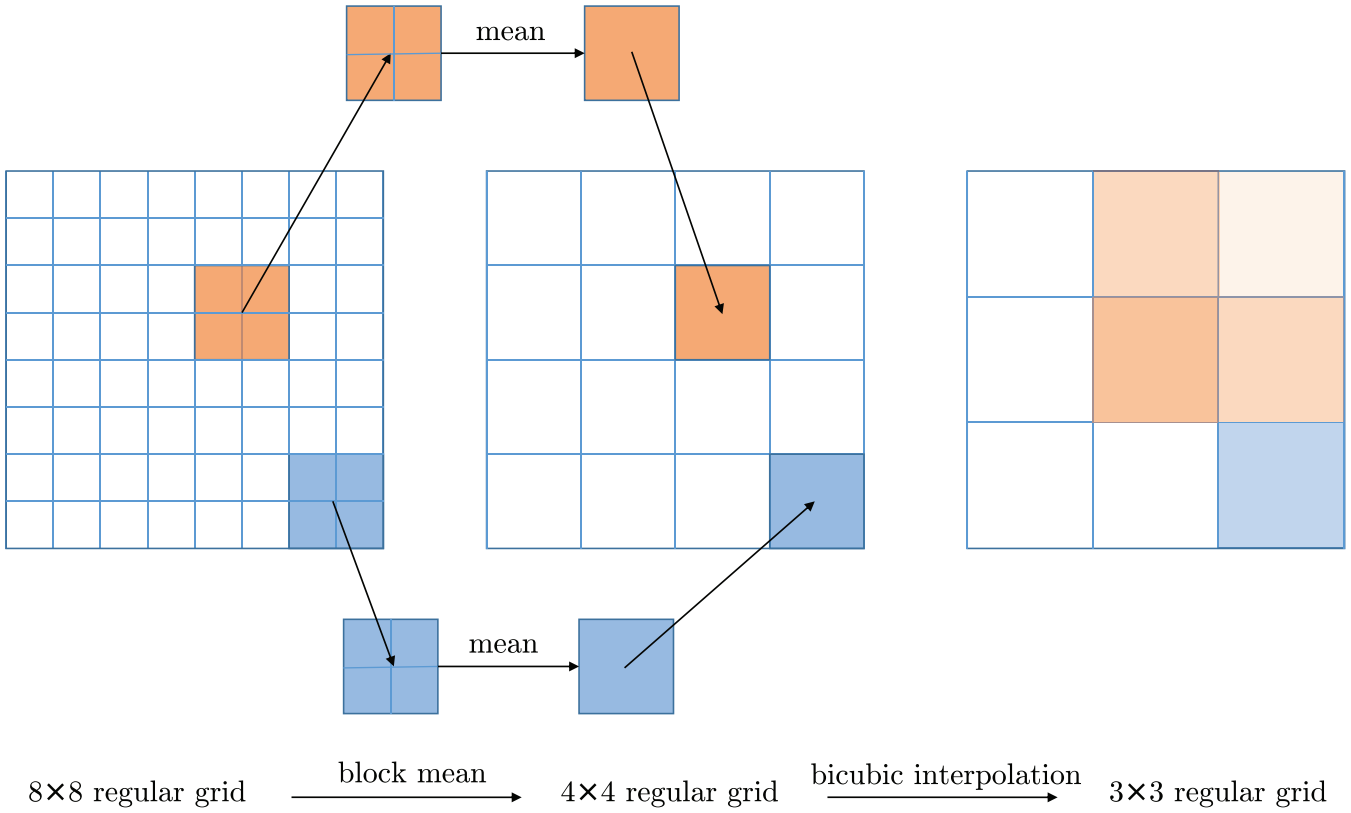

Figure 2. Pictorial example of adaptive downscaling from an 8 × 8 grid to a 3 × 3 grid. The leftmost grid (8 × 8) contains some sparse data, represented by the orange and blue blocks; firstly the resolution is reduced to the closest divisor of the original that is higher than the target (here 4 × 4, as 4|8 and 4 ≥ 3). We then use a two-dimensional interpolation method to downsample from this intermediate resolution to the final 3 × 3 grid.

Centre for Medium-Range Weather Forecasting, an atmospheric global 4D-Var reanalysis from 1979 to the present. This is available at T255 spectral resolution (i.e. a comparable spatial resolution to N256, using Table 2) with 60 vertical levels, 27 of which are below 100 hPa, at six-hourly temporal resolution. For ERA-I, these output vertical levels are identical to the model vertical levels. We also make use of the Tropical Rainfall Measuring Mission (TRMM) multi-satellite surface precipitation product (3B42; Huffman *et al.*, 2007), which has 0.25° × 0.25°, 3-hourly resolution, and global coverage between 50°N and 50°S; this is available from 1997, and is calibrated and merged with a selection of other IR satellites: Geostationary Meteorological Satellite (GMS), GOES-East, GOES-West, Meteosat-7, Meteosat-5, and NOAA-12.

3. Propagation and duration

The NWP models at each resolution for each case-study were run for seven days, which is substantially longer than any of the MD durations given in Table 1. The previously described tracking algorithm was applied to the output data to determine whether an MD was present in the forecast and, if so, what its track was. In all 56 forecasts (seven case-studies at eight resolutions each), an MD of sufficient length not to be dismissed as a transient feature was detected. Examples of tracks from two case-studies, along with the overall averages are shown in Figure 3, the average tracks (in bold) are computed from normalized durations (that is to say, if one had two MDs of duration 48 and 60 h, the halfway point of the average track would be taken from the coordinates at 24 and 30 h respectively). Also given in the figure are the official tracks from the IMD (grey) and as computed from ERA-Interim reanalysis (black). The two case-studies given are a longer westward system that terminated on the west coast and another propagating northward that terminated over Bangladesh, from the 16 September 2015 and 20 June 2015 experiments respectively. It is evident from the two examples and the seven-member multi-depression mean shown in Figure 3 that increasing the resolution improves the track forecasts: the genesis/termination points, durations, and along-track coordinates all tend towards greater accuracy. We can look at the forecast track accuracy more quantitatively by normalizing the track lengths and computing the mean distance error compared to the IMD or ERA-I tracks; i.e. we consider a given lifetime percentage and for each resolution calculate the mean distance between its tracks and the 'truthful' ones. This is done for each resolution, tested against both IMD and ERA-I tracks, and the results are given in Figures 3(a) and (b) respectively. We see that the errors generally grow with time, with N96 performing particularly poorly. Regardless of whether the comparison is made with ERA-I or IMD tracks—although it strictly ought to be the former—it is evident that, above N216 resolution, error reductions become more marginal in terms of track position.

4. Representation of the monsoon trough during depressions

To understand the relationship between model, resolution, and depression, we must first consider the environment in which depressions are embedded: the Indian monsoon trough. It is a favourable environment for MDs, a low pressure area with large moisture fluxes, wrapped in lower-tropospheric cyclonic winds, all three of which tend to strengthen during the passage of a depression (Hunt *et al.*, 2016a). Thus, the discussion of the nature of a depression-trough[†] in models and its sensitivity to resolution is an important part of a clear analysis of MDs in NWP models.

4.1. Rainfall

Figure 5 shows a comparison of mean rainfall across the case-studies for a range of resolutions with each other and the TRMM 3B42 surface precipitation product for the same period. We

[†]We shall hereafter use the term *depression-trough* to refer to the trough when it is co-existent with a monsoon depression.

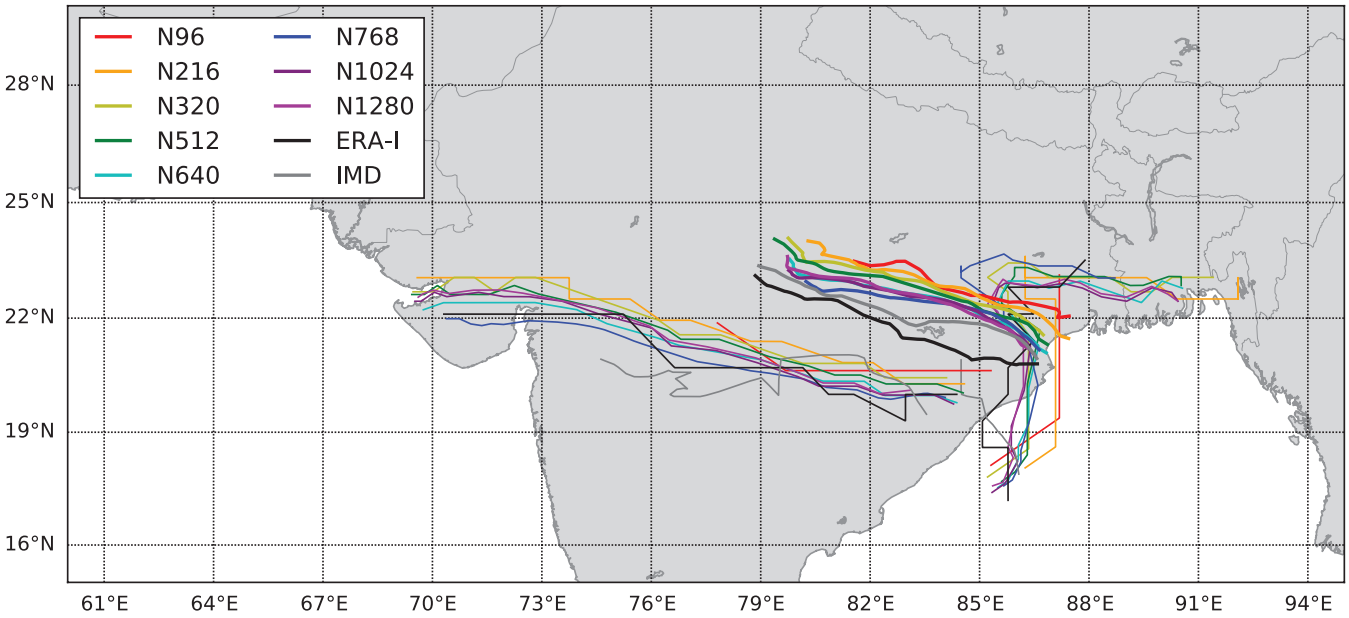

Figure 3. A selection of tracks from the case-study experiments. In bold are the mean tracks for each resolution, normalized by duration; the westward propagating tracks that traverse the peninsula are from the 16 Sep 2015 MD, and those propagating northwards toward the Ganges Delta are from the 20 Jun 2015 MD. In black are the tracks computed from ERA-Interim, and in grey are the official IMD tracks.

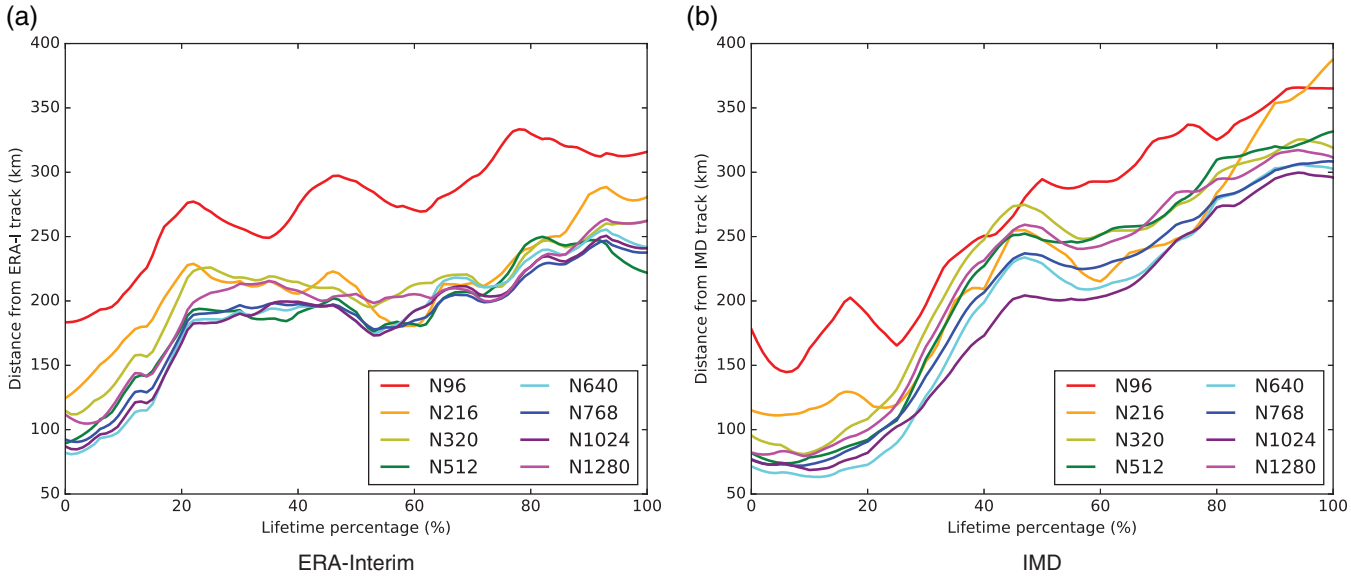

Figure 4. Mean distance from (a) ERA-Interim track and (b) IMD track as a function MD lifetime percentage. Duration normalization is carried out before averaging, as in Figure 3.

see that increasing the resolution consistently does two things to the mean picture: it reveals a more complex structure, and results in generally higher maximum rainfall rates. Naïvely, we might say that these can be explained directly by considering how the fields are represented–finer detail simply cannot be depicted at the lower resolutions, since there are not enough pixels, and the highest rainfall rates have very small spatial scales and thus tend to get smoothed as resolution is reduced. However, this is not the complete story: the structure becomes more filamental[‡] with increasing resolution, providing evidence that finer mesoscale processes are being represented in the model (whether or not they exist in reality); further, both the mean rainfall in the trough and the frequency of 'very heavy' rainfall events, officially defined by the IMD as rates of 125 mm day^{-1} or greater, also increase with resolution. Figure 6 gives a depiction of the latter: the fraction of time steps where a MD was considered present in ERA-Interim (for the relevant range of dates) in which the model/TRMM 3B42 determined that very heavy surface precipitation was present. We see that the frequency of such events in the trough increases with resolution, tending towards the values suggested by TRMM, however the orographic representation over the Western Ghats and across western Indochina remains poor throughout (for example, precipitation predicted by the model over the Western Ghats is too frequent, too weak, and in the wrong location), and this is important to quantify because the rainfall over the mountainous west coast is heavily modulated by the presence of MDs (Hunt *et al.*, 2016a). The lower-tropospheric cyclonic circulation associated with a typical MD strengthens the monsoon westerlies over the Western Ghats, increasing the associated orographic rainfall. It is also evident that, while the forecast frequency of heavy rain improves with resolution, the total amount of rain associated with the MD becomes a clear overestimate when compared to TRMM; and across all resolutions, the model tends to constrict the spatial scale of heavy rainfall events to be closer to the MD centre. Note also the footprint of a disturbance in the Arabian Sea contemporaneous with the June 2015 disturbance; it is included in these maps of the composite depression-trough,

[‡]i.e. it is anisotropic, which we would not expect if this detail came about solely as a result of having a 'sharper' image.

but will be excluded from depression composites in subsequent sections.

We can interrogate the bulk rainfall statistics a little more by looking at a histogram of precipitation rates in the depression trough; unfortunately it is difficult to compare individual events due to the individual storms being typically smaller than the forecast track errors. This is done across all case-studies (using dates from ERA-I tracks), giving over 160 time steps. For a simple definition of the trough (20–25°N, 75–85°E), the histograms are shown in Figure 7. The distributions from TRMM 3B42[§] and the model at all resolutions are significantly different, although from resolutions of about N512 upwards (even after downscaling), the model is capable of representing the higher rainfall rates that TRMM suggests exist there. There are three distinct regimes with boundaries at approximately 125 mm day^{-1} (coincidentally) and 500 mm day^{-1}. In the low-rate regime, we see that, regardless of resolution, the model overestimates the frequency (by as much as an order of magnitude as the 0.1 mm h^{-1} resolution of TRMM 3B42 is approached). This exaggerated drizzle is a well-known issue in global models (e.g. Dai, 2006; Stephens *et al.*, 2010). This is compensated for by an under-representation of higher rainfall rates in the model, although above about 225 mm day^{-1} this sharply improves with increasing resolution. In the very-high rate regime, resolutions below N512 produce nothing, whereas N512 and above tend to overestimate the frequency and amount; however this should be taken with the caveat that these events are rare (of the order of two or three over the total dataset of each resolution).

4.2. *Synoptic circulation*

It has been shown that mid-tropospheric relative humidity is an important factor in the modulation of MD genesis (Ditchek *et al.*, 2016), that MDs are capable of organizing mid-tropospheric circulation that is absent in the climatology (Hunt *et al.*, 2016a) and, further, that fields at these altitudes are thermodynamically coupled to precipitating events at the surface (Hunt and Turner, 2016; Hunt *et al.*, 2016b). Bearing this in mind, Figure 8 shows the mean 500 hPa depression-trough relative humidity and winds for a selection of resolutions, with that from ERA-Interim (for the same dates) for comparison. The relative humidity at this altitude is consistently over-estimated by the model (typically 5–10% in the trough), but this improves with increasing resolution. We also note that the maximum relative humidity moves south (towards that observed in ERA-I) with increasing resolution; this is likely to be at least related to the tracks having lower latitude (cf. Figure 3). The circulation is well represented at all shown resolutions, although in the model it is more convergent (not shown, though inferable from Figure 8) over the trough than in the reanalysis, and this is exacerbated by a resolution increase; it is perhaps important to note that this is correlated with an increase in the average precipitation for the region.

The circulation at 700 hPa, shown along with potential vorticity (PV) in Figure 9 looks similar to that at 500 hPa, with the exception of the strong monsoon westerlies south of the disturbance. At low resolutions, the trough PV is displaced (too far to the northeast), but this improves with resolution, perhaps indicating a better representation of the known axial tilt in MDs. We also note that the PV over the Arabian Sea and near the high orography in Pakistan is severely overestimated at all resolutions, when compared to the reanalysis.

Summarizing, we have seen that an increase in model resolution is correlated with an intensification of activity in the depression-trough: an increase in moisture, stronger circulation, and associated higher rainfall rates. Therefore we should expect that increasing resolution should also be correlated with stronger MDs. However, the impact of increasing resolution is small once we get beyond N320.

5. Evaluation of composite depression structure

Now that we have explored in some detail the sensitivity of a depression-trough to changes in horizontal model resolution, we shall look at the performance of the models from an MD-centred point of view. This is simply done via the construction of a composite, which has been done before for, e.g. tropical cyclones (Catto *et al.*, 2010) and monsoon depressions in observations (Godbole, 1977; Keshavamurty *et al.*, 1978; Sarker and Choudhary, 1988; Prasad *et al.*, 1990) and reanalysis (Hurley and Boos, 2015; Hunt *et al.*, 2016a). Simply put, the composite is composed by taking all depression-time steps, centring the data for the field of interest on the depression centre, and then taking the average. The Appendix gives a formal description.

One simple method, commonly used in the context of tropical cyclones, to overview the system-relative composite is to examine the extreme values of intensity-related variables as a function of resolution, averaged over the case-studies. Figure 10 shows the appropriate extreme (or mean) values for surface pressure, 350 hPa temperature anomaly, total precipitable water (TPW), and free convective depth; the values are computed from a 1000 km-sided box surrounding the centre, with blue dots marking the values from individual case-studies and the blue line their average. The green line in each subplot marks the mean value from the ERA-I tracks and all fields are interpolated to N216 for comparison using the algorithm outlined in section 2.5, which is an important step to undertake when performing intercomparison of extreme values across differing resolutions. The first field under consideration (Figure 10(a)) is the lowest central surface pressure associated with the MD during its lifetime: parallel to similar studies for tropical cyclones (e.g. Strachan *et al.*, 2013) we see that increasing the resolution strengthens the minimum surface pressure associated with the system irrespective of appropriate downsampling, though unfortunately even at some of the lowest model resolutions (N216: 989.7 hPa), it is still lower than the values suggested by ERA-I reanalysis, and deepens substantially beyond this (N1280: 984.8 hPa). During our discussion of representation of the depression-trough in the MetUM (e.g. Figure 9), we initially suspected that MDs may be more intense in the model than in reality, and this corroborates that analysis.

We know that MDs are largely in thermal wind balance with the latent heat-induced warm core aloft, and that the highest temperature anomalies are found at around 350 hPa, so this is an important metric to consider when discussing intensity; Figure 10(b) shows the maximum values of the 350 hPa temperature anomaly (Figure 13 and associated discussion give an explanation of how the climatology is generated for the MetUM). This is handled far better than surface pressure by the MetUM, where the predicted values of approximately 9.5 K in the models at higher resolution is insignificantly separated from the ERA-I value of 8.7 K; and this accuracy generally improves with increasing resolution, especially beyond N320. However, it is still clear that these extremes are too high at all resolutions.

Latent heat release in the troposphere is strongly coupled with the moisture presence, and so we turn our attention to a good proxy of this: TPW. Figure 10(c) shows the mean values of column TPW in the aforementioned–1000 km sided, surrounding MD centre–box across the resolutions; this again is improved (compared to reanalysis) by increasing resolution from 66.3 mm at N96 to 64.3 mm at N1280, however the degree of improvement is marginal when compared to the overall error against the reanalysis value of 60.9 mm. So, the model asymptotically tends to roughly a 5% overapproximation of the total mass of water in the atmosphere surrounding the MD. This is not due to a temperature discrepancy (as we have briefly seen earlier in this section and will confirm later on examination of the

[§]Recall the resolution of TRMM 3B42 roughly equates to N720

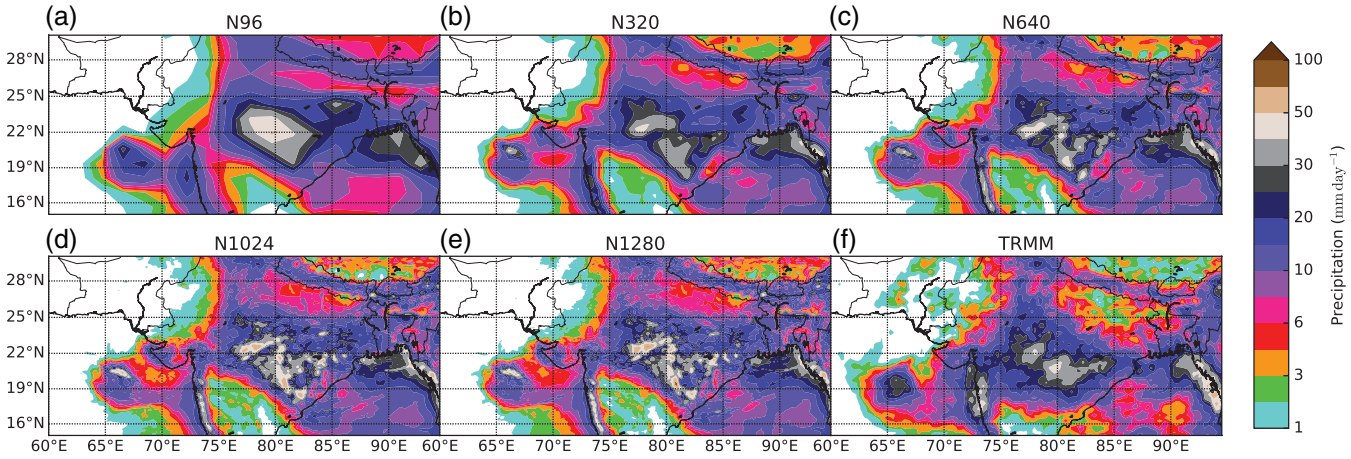

Figure 5. Mean precipitation (mm day^{-1}) in the monsoon depression-trough and surrounding area for five resolutions (a) N96, (b) N320, (c) N640, (d) N1024, (e) N1280, compared against (f) the same period(s) for TRMM-TMPA 3B42. Each is averaged over the same set of dates and times, i.e. those in which a MD was considered present in ERA-Interim by our tracking algorithm.

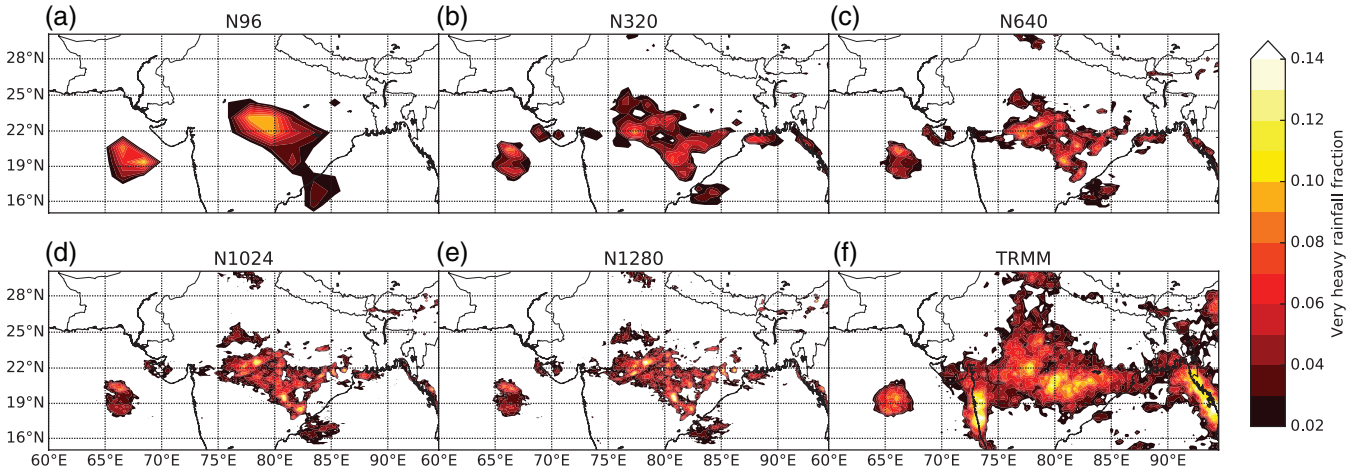

Figure 6. Fraction of total time for which 'very heavy' rainfall events were present in the depression-trough for the resolutions as in Figure 5, compared against the same period(s) for TRMM-TMPA 3B42. 'Very heavy' is defined by the IMD as rates exceeding 125 mm day^{-1}. The computation is as in Figure 5.

vertical profile of temperature), there is simply more moisture being put into the troposphere. This corroborates the behaviour of the trough that we saw in Figure 8, and is not a problem generally found in the tropics (Martin *et al.*, 2006), so we can fairly safely assume there is something special about the representation of monsoon depressions that is causing this.

We extend this discussion a little further by considering the changes in tropospheric stability associated with the depression. For this, a good proxy is CAPE, although as we will come to see, it is rather too noisy to use when looking for extreme values. Instead, we consider free convective depth, the difference in altitude between the level of free convection and the level of neutral buoyancy; the larger this value, the more latent heat can theoretically be deposited throughout the troposphere. The maximum values for this are shown as a function of resolution in Figure 10(d), and we can immediately see a rapid improvement with increasing resolution, tailing off at about N512 where the mean maximum free convective depth of 15.56 km compares favourably to the reanalysis value of 15.63 km. Clearly, then, the issue of too much moisture and over-intensification of the vortex does not appear to be related to atmospheric stability. This is one of a great many features affected by the convective parametrization scheme, which in part explains its overall improvement with resolution.

5.1. *Vertical structure*

Monsoon depressions involve a number of complex, moist thermodynamic processes occurring over irregular orography and land surface type that result in characteristic vertical structure that has been qualified in some detail by previous authors (Godbole, 1977; Hurley and Boos, 2015; Hunt *et al.*, 2016a). One consistent, common feature in the vertical structure is a bimodal PV core: a maximum at ∼500 hPa primarily caused by the upper-tropospheric warm core, and one at ∼700 hPa primarily caused by the lower-tropospheric relative vorticity maximum. South–north cross-sections across the composite PV for MDs at each resolution, as well as those derived from the ERA-I and IMD tracks using ERA-I reanalysis, are shown in Figure 11. The bimodal structure itself is clearly well captured across the range of horizontal resolutions, although the magnitude of the maxima is too great by as much as 50%. This error is essentially consistent across the resolutions (with the exception of N96) which is apparently contradictory to recent work (Roberts *et al.*, 2015) that suggests tropical cyclone intensity and horizontal model resolution are strongly correlated, although their study is a climate run with several hundred events (i.e. the cyclones spin up from the model rather than initial analyses). We note here that the MetUM model output was made to match the vertical levels available as ERA-I output data–24 levels between 1000 and 150 hPa (approximately 200 m resolution in the PBL, decreasing to 2 km at the tropopause).

Since both maxima in PV are significantly overestimated by the model, we should expect this to be reflected in the primary contributors to each. We shall start by looking at the distributions of lower-tropospheric relative vorticity as a function of resolution. Now, we cannot be certain, although it is likely, that the vorticity maxima (climatologically found at the centre at 850 hPa) will necessarily be at the tracked MD centres–MDs are not strictly

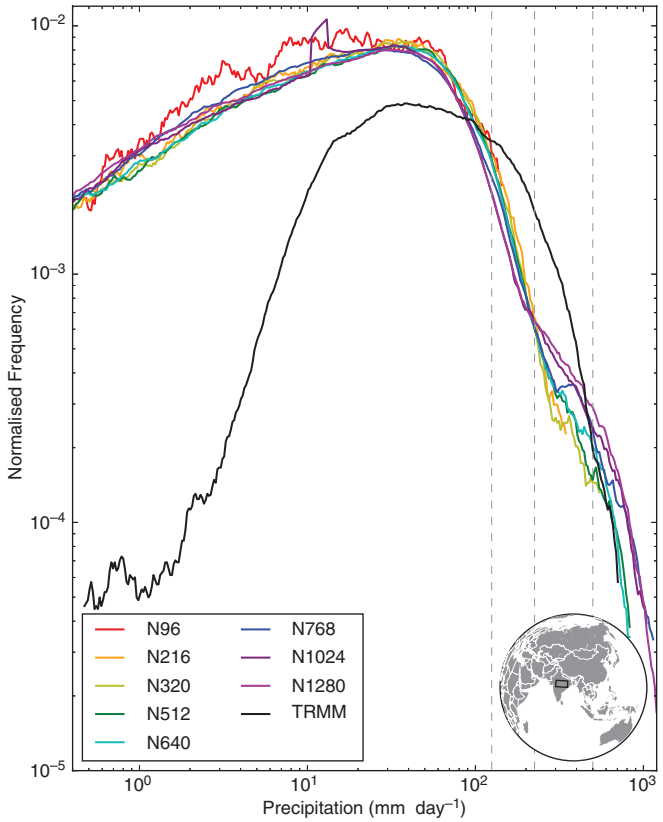

Figure 7. Normalized log-histogram of precipitation (mm day^{-1}) in the depression-trough during the case-study MDs. Here, the trough is defined simply as a box (see inset map) 20–25°N, 75–85°E. Breaks in lines indicate zero counts. Vertical dashed lines are shown for values of 125, 225, and 500 mm day^{-1}.

line vortices (Hunt *et al.*, 2016a), and they tilt westward with height (Godbole, 1977); so, to capture the values associated with the vortical core, we take all relative vorticity values in a prescribed cuboid of length 400 km centred on the MD centre with vertical extent 925–750 and 650–300 hPa. All values within these cuboids are taken for all times where an MD is present in any of the case-study data and collected into histograms, which are given in Figure 12. Although these data were coarsened to T255 resolution (lower than this was undesirable because it leaves data sparse in the domain used), the lower resolutions were found (using a broader domain) to be insensitive to downsampling. We note that all histograms closely resemble the gamma function, and that increasing resolution causes increased positive skewness with diminishing return; this indicates an increasing variance which is not reflective of the distributions found for reanalysis MDs (grey and black in Figure 12). There is also a gain in intensity with increasing resolution until N512; this is more apparent in the mid-tropospheric sample of Figure 12(b) where we also see the model performs substantially more poorly by overpredicting the MD intensity. Had we not opted to downsample the data from higher resolutions before producing the histograms, we would have recovered (not shown) a figure much like Figure 8 of Strachan *et al.* (2013). We note that on statistical tests of these distributions at both levels, the three lowest resolutions were each significantly different from each other at the 99% confidence level, as well as from the five highest and the IMD/ERA-I tracks (the two latter sets were also significantly different from each other at this level, although the members of each set were not individually significantly different from each other). The differences in intensity prediction between the two altitude segments shown in Figures 12(a) and (b) are important: this is a first indicator that a primary cause of the model's failings is rooted in the upper/mid-troposphere.

MD structure in the upper/mid-troposphere is strongly influenced by latent heat release there, so the next logical step is to examine the vertical thermal structure of depressions. This, in the form of temperature, is given for each resolution, with the ERA-I and IMD track composites for comparison, in Figure 13. Since perturbations to the temperature caused by MDs are roughly two orders of magnitude smaller than the vertical gradient through the troposphere, we look at the temperature anomaly, rather than the raw temperature field. For composites computed from both model output and reanalysis data, the anomaly was computed by subtracting the short climatology from the total forecast period (37 days over the seven MDs); this is realistically too short a period to conduct a sound analysis (climatologically, one would expect one or two MDs in a period of this length), although comparison of the ERA-I/IMD composites with other vertical thermal composites (e.g. Godbole, 1977; Hunt *et al.*, 2016a) indicates that they are fairly representative. In the model, the magnitude of the warm anomaly in the mid-troposphere increases with resolution until N320; at resolutions thereafter the warm anomaly remains approximately constant. In contrast, there is little difference between the boundary-layer cold anomalies in any resolution, other than perhaps a more defined structure with increasing resolution. Comparing the composite structure from the models to those from the reanalysis, it is evident again that the MD intensity is overestimated. Not only are the warm anomalies aloft roughly 0.25 K too strong, but they are significantly elongated in the vertical, extending up to a kilometre higher than in the reanalysis. Conversely, the cold anomaly near the surface is well-represented in both magnitude and shape at all resolutions, arguably being slightly too confined to the centre.

We shall conclude this particular discussion with an exploration of the vertical wind structure given in Figure 14 which is also presented as an anomaly so as to remove the effects of the monsoon jets. As expected, the structure is asymmetrical with wind speed being substantially higher north of the centre than south. The MetUM captures this asymmetry at all resolutions, and matches the intensity of the weaker lobe in the reanalysis composites whilst overestimating the intensity in the stronger lobe. We also note a deeper circulation: the model has a well-established mid-tropospheric cyclone that is all but absent in the reanalysis, likely coupled with the stronger and deeper latent heat release seen in Figure 13. Again, once the resolution is increased beyond N320, no significant changes in structure or intensity are noted in the composite.

Summarizing the composite form, we have seen that, in an NWP set-up, the MetUM generally captures the spatial structure of monsoon depressions well,[¶] improving with resolution until about N512; however, the intensity is typically overestimated, increasing with resolution early on until saturation at N320. We remark at this stage the caveat of having a relatively low-resolution reanalysis (i.e. one that falls between N216 and N320); the only thing we can say with certainty is that the composites at N216 and N320 are too intense and that this bias appears to worsen with resolution, but this cannot be properly verified without higher-resolution observational/reanalysis data. In the mid-troposphere, this is explained by an increase in the frequency of events of greater intensity (saturating at N320); in the lower troposphere this is exacerbated by a shift also in the mode.

5.2. *Horizontal structure*

Quantifying horizontal structure of MDs is also important: at the surface, interaction of the synoptic flow with local orography and sharp gradients in land type supports complicated, asymmetrical structure both there and aloft. One of the most strongly affected, and important, variables in this context is surface precipitation, so we shall start the discussion there. Figure 15 shows composite surface rainfall for the case-studies at each of the eight resolutions

[¶]However, we must note that this is in the specific case where we have initialized the model quite close to the start date, as one would do in forecasting. We make no assertions about how a climate model would perform, particularly once biases develop in the atmosphere.

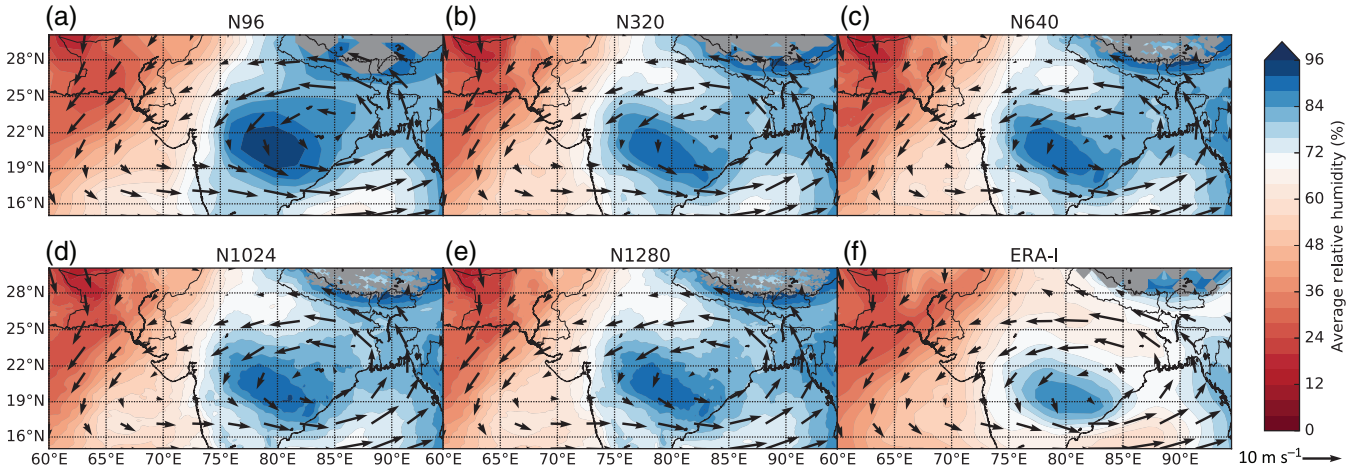

Figure 8. Mean 500 hPa relative humidity (colour shading) and 500 hPa winds (arrows) in the monsoon depression-trough and surrounding area for (a)–(e) the same resolutions as in Figure 5, compared against (f) the same period(s) for ERA-Interim. The computation is as in Figure 5.

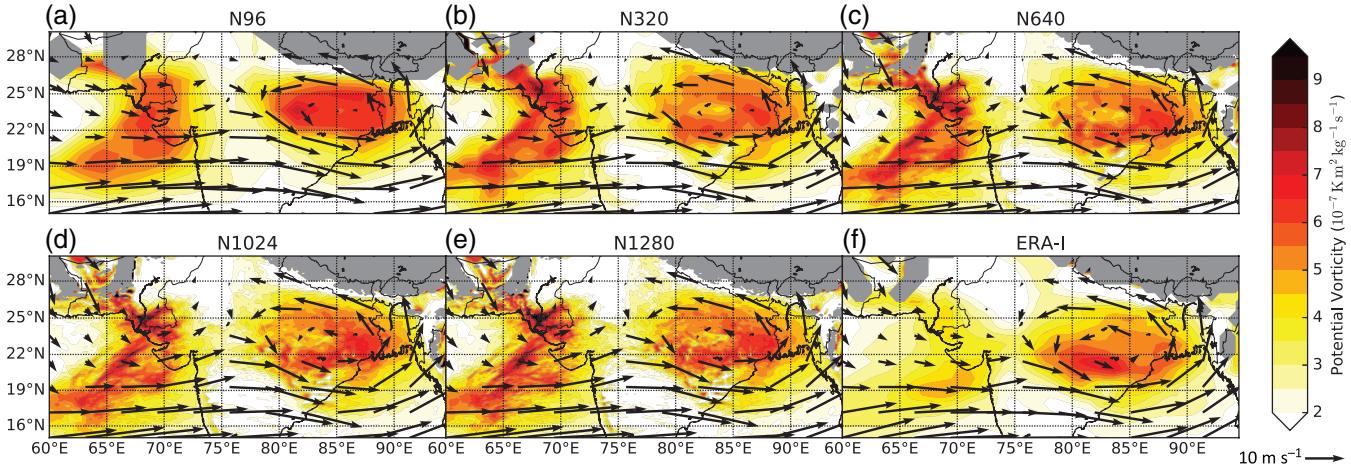

Figure 9. Mean 700 hPa potential vorticity (colour shading, 10^{-7} K m^2 kg^{-1} s^{-1}) and 850 hPa winds (arrows) in the monsoon depression-trough and surrounding area for (a)–(e) the same resolutions as in Figure 5, compared against (f) the same period(s) for ERA-Interim. The computation is as in Figure 5. Where orography is above 700 hPa, grey shading is shown.

considered in this study, with equivalent computations based on the ERA-I/IMD tracks, taking precipitation data from TRMM 3B42. One of the most apparent features follows directly from inspection of the behaviour of rainfall in the monsoon trough in general (Figure 5), i.e. that the model at all resolutions tends to produce smoother, more coherent patterns. Increasing resolution produces finer spatial features that slowly tend towards the observational structure, and causes an increase in the values associated with the near-central maximum. In combination, these result in finer resolutions seemingly producing ever higher fidelity results when it comes to rainfall. However, there are a few systematic problems across the spectrum of model resolutions, some of which we have already noted while discussing representation of the trough: orographic rainfall in the southwest (Western Ghats) and northeast (Himalayan foothills) is consistently overestimated, although this does improve slightly in the northeast with increasing resolution. Inspection of the data (not shown) suggests that the model has a tendency to produce constant low rain rates at these locations which is not reflective of reality; further, the rain shadow to the south, which is not so immediately obvious in Figure 5 generally has too much precipitation, something that gets worse with resolution until N1280. Of course, these specific failings are not directly linked to the presence of an MD; the orography is there regardless of the state of the trough, but it is known, for example, that MDs increase (decrease) rainfall along the Western Ghats (Himalayan foothills) by as much as 15 mm day^{-1} (Hunt *et al.*, 2016a), and based on what we have seen so far, it seems unlikely that this would be well represented given the poor spatial structure and intensity seen (particularly over the Ghats) in Figures 5 and 6.

We can use other diagnostics to pick apart the precipitation structure, and it would be appropriate to select these based on the salient pretence that they ought to represent contrasting factors: for example, the amount of water available in the column and the ability of the column to rain out this water, for which TPW and CAPE respectively are suitable proxies. Figure 16 gives the composite (horizontal) structure of TPW (mm) and CAPE (J kg^{-1}) across all resolutions and for ERA-I/IMD tracks in ERA-Interim data. These are presented such that darker block contours represent higher CAPE values and redder line contours represent higher values of precipitable water. At first glance, we see that the model has a tendency to overestimate TPW and underestimate CAPE in the vicinity of the MD centre. In terms of quantity, these errors appear to mostly cancel each other out when it comes to the precipitation composite, and although CAPE is only a proxy (if it is indeed even that) for convective rainfall, we shall see later that the majority of rain associated with the MD in the model can be attributed to convective events. In terms of spatial structure, the TPW is fairly well represented: the central maximum is arguably pushed slightly too far from the centre, particularly in the lower resolutions, but this is certainly recovered at resolutions upwards of N768; the MetUM appears to do a fairly poor job over the Tibetan plateau, and it is worth noting here that these 'parcel ascent' variables were computed from the conditions at the local surface, starting from the orographic height. However, this failure does not have a significant spatial reach, as TPW values become rapidly comparable to those given by the reanalysis beyond the foothills. Conversely, the spatial distribution of CAPE in the model composites is quite different to that suggested by the

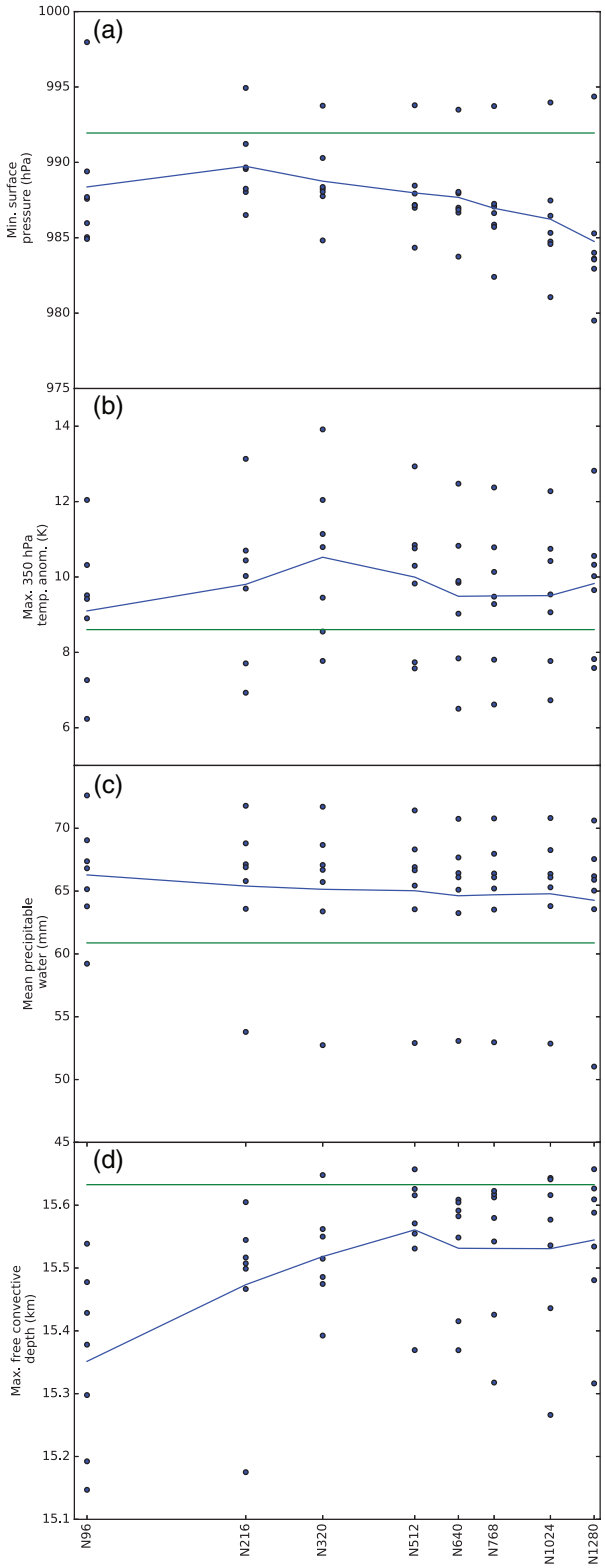

Figure 10. A selection of intensity diagnostics as functions of resolution. (a) Minimum surface pressure obtained (hPa), (b) maximum temperature anomaly (K) at 350 hPa relative to climatology, (c) mean total column precipitable water (mm), and (d) maximum free convective depth (km). Each is computed from a 1000 km-sided box surrounding the centre, with the value for each MD case-study; these individual values are plotted as blue circles at each resolution with the mean given by the blue line. The green line represents the value obtained by performing the same computation on the ERA-I track. Here, free convective depth is defined as the difference in altitude between the levels of free convection and neutral buoyancy.

analysis. For the sake of clarity, we note that this is computed at each time step and then composited, i.e. it is the composite of the CAPE, as opposed to the CAPE of the composite. Across resolutions, the MetUM has a tendency to place the maximum CAPE (associated with the MD) several hundred kilometres too far to the northwest, such that it no longer really has an overlap with the MD centre. We also note that values over the ocean (far southeast) are overestimated, and values over the Himalayan foothills (near northeast) are generally underestimated.

5.3. *Cloud structure*

Now, having looked at precipitation and related fields in some detail in the horizontal, we turn our attention to cloud. Cloud cover is important in the context of a depression for a number of reasons. Firstly, it plays an important part in governing the thermal and diurnal structure–radiative cooling at the top caps the warm thermal core aloft and sets up the static instability at night that is responsible for enhanced precipitation at the surface, and it serves to block insolation near the centre causing the cold thermal core at the surface. Secondly it has long been thought that convective instability of the second kind (CISK; Charney and Eliassen, 1964) is at least in part responsible for the intensification of MDs (Krishnamurti *et al.*, 1975; Sikka, 1977; Keshavamurty *et al.*, 1978; Shukla, 1978; Chen *et al.*, 2005). That having been said, any cross-section of a composite field that is fundamentally binary is limited in what it can tell us; however, we can use combinations of colour to represent three variables simultaneously. We can use this in conjunction with the model/reanalysis output fields of low-/mid-/high-level cloud cover which assess the fractional cloud amount between two pre-defined heights. For both the MetUM output and ERA-Interim, these heights are defined on sigma levels that correspond to (from the surface):

$$\text{low} < 1.8\,\text{km} \leq \text{mid} < 5.5\,\text{km} \leq \text{high} < 13.7\,\text{km} \qquad (2)$$

for the MetUM and

$$\text{low} < 1.9\,\text{km} \leq \text{mid} < 6.3\,\text{km} \leq \text{high} \qquad (3)$$

for ERA-Interim. Figure 17 shows the composites for these variables across model resolutions (and for ERA-I/IMD tracks) displayed in colour space: that is to say, if each of low-/mid-/high-level cloud cover have a range of 0 to 1, and we define coordinates in RGB colour space, (R, G, B) such that (0, 0, 0) is black and (1, 1, 1) is white, then we can represent cloud cover by the unique colour coordinate (C_L, C_M, C_H) where C_L, C_M, and C_H are low-/mid-/high-level cloud cover fractions respectively; thus, for example, full low-level cloud cover with nothing above it would be represented as pure red. Looking at Figure 17(a) with this in mind, we see a common structure emerging across the resolutions and in the reanalysis composites: full cloud cover extends for several hundred kilometres southwest of the centre, and conversely, low-level cloud dominates in the northeast quadrant. There is also ubiquitous high-level cloud, along with a mix of all types over the Himalayas in the far northeast. This overview agrees with the CloudSat-derived composite produced by Hunt *et al.* (2016b), which suggested deep cloud persisted south of the centre, transitioning to lighter, lower-level cloud in the north with stratus and altostratus over the Himalayas. Unusually, there are few differences across the resolutions when it comes to spatial distributions or even magnitudes: the axis separating deep cloud and low-level cloud rotates from north–south at lower resolutions, and finer structure becomes apparent, including traces of individual squall lines and rain bands. These compare fairly well to the reanalysis composites (even given the different classification boundaries between the two sets of products) although there are some subtle differences: the deep cloud cover to the southwest of the centre is weaker than suggested by the MetUM composites, and tends to be elongated and wrapped around the centre, as opposed to being roughly isotropic with a well-defined maximum; and the Himalayas are handled differently, but since these are purely modelled products (even in the reanalysis), it is likely inconsequential.

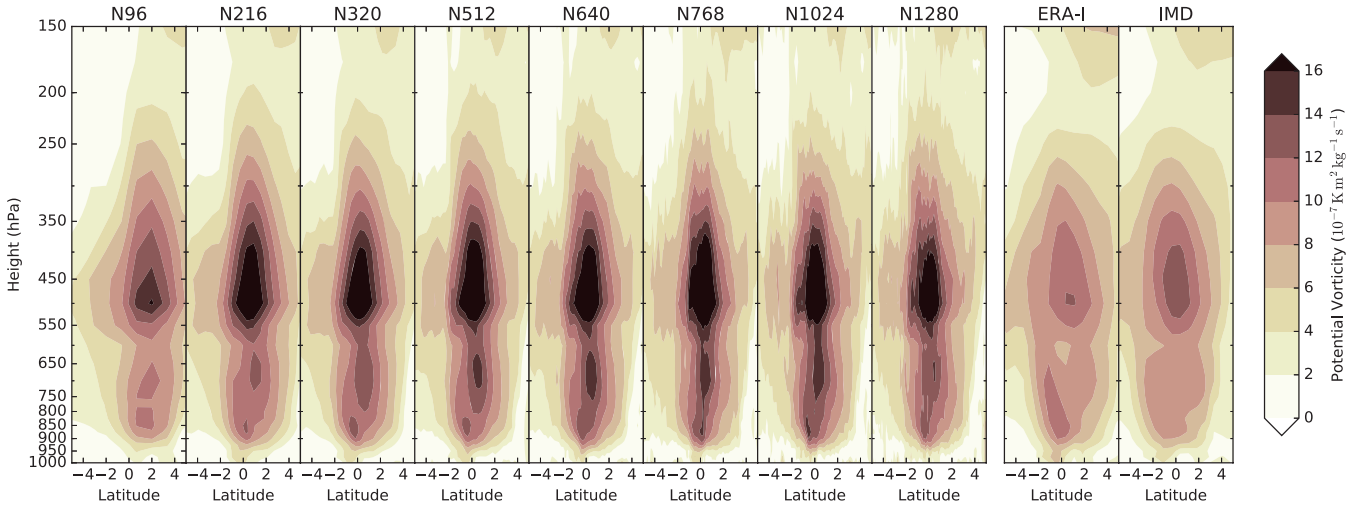

Figure 11. Mean composite potential vorticity (10^{-7} K m^2 kg^{-1} s^{-1}) for the case-study MDs. Tracked MDs in the forecasts and reanalysis are centralized such that their centres lie at the origin of the composite. Here, south–north cross-sections through the composite origin are presented for all resolutions, and the composites derived from both our ERA-I tracks and the IMD tracks (i.e. the tracks determined from ERA-I and those given by the IMD, both applied to ERA-I data–see text for more details). The ERA-I equatorial resolution of ∼78 km is approximately N256.

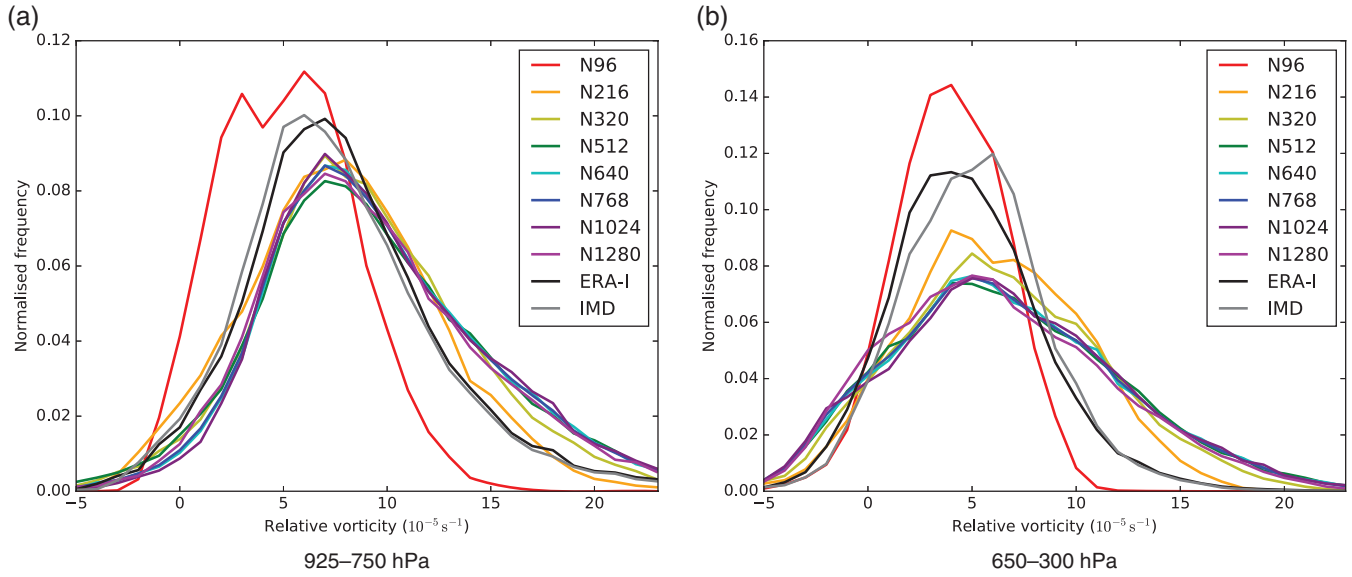

Figure 12. Normalized histograms of relative vorticity (10^{-5} s^{-1}) for each resolution and the ERA-I and IMD tracks. These are taken at all times where an MD is present, from a cuboid of horizontal length 400 km centred on the origin, and vertical extent (a) 925–750 hPa and (b) 650–300 hPa.

$$P(x,y) = P_{\text{residual}}(x,y) + \sum_{n=0}^{1} A_n \exp\left(-\begin{bmatrix} x-x_{o,n} & y-y_{o,n} \end{bmatrix} \times \begin{bmatrix} \frac{\cos^2\theta_n}{2\sigma_{x,n}^2} + \frac{\sin^2\theta_n}{2\sigma_{y,n}^2} & \frac{\sin 2\theta_n}{4\sigma_{x,n}^2} - \frac{\sin 2\theta_n}{4\sigma_{y,n}^2} \\ \frac{\sin 2\theta_n}{4\sigma_{x,n}^2} - \frac{\sin 2\theta_n}{4\sigma_{y,n}^2} & \frac{\sin^2\theta_n}{2\sigma_{x,n}^2} + \frac{\cos^2\theta_n}{2\sigma_{y,n}^2} \end{bmatrix} \begin{bmatrix} x-x_{o,n} \\ y-y_{o,n} \end{bmatrix} \right) \quad (4)$$

5.4. *Diurnal cycle*

The diurnal cycle of Indian monsoon depressions was first characterized and detailed by Hunt *et al.* (2016b) using observations from TRMM 3B42. They showed that two strongly varying modes of differing spatial scales existed almost in antiphase, and that these could, together, be simply modelled as the sum of two arbitrarily phased Gaussians (Eq. (4)). P is the observed spatial distribution of the precipitation, P_{residual} is the difference between the observed rainfall and the fitted function, n is an index for the two Gaussian functions, σ_x and σ_y refer to the standard deviation of the Gaussian along the x and y axes respectively, (x_o, y_o) are the coordinates of the centre of the Gaussian, and θ is its rotational phase. These functions were then fitted to diurnally separated data (by which we mean composites of 0000, 0300, 0600, . . . , 1800 UTC) to recover the two distinct modes: an outer mode peaking at dusk with small magnitude and large scale, related to the tropical convection cycle over land, and a central mode peaking at dawn with large magnitude and small scale, related to the radiation-induced instability in the column. We now repeat the analysis of Hunt *et al.* (2016b) across our range of resolutions to determine to what extent the MetUM is capable of capturing the diurnal cycle, and how resolution affects it. The maximum and minimum values of the amplitude coefficients, A_n, (mm h^{-1}) for each mode and each resolution are given in Table 3, along with their respective times (to the nearest 3 h, representative of the model output temporal resolution). We see that the central mode is very well captured from N512 upwards (though a little too intense), but the outer mode is rather poorly represented–both in being far too weak, and in getting the timings entirely incorrect. The failure of the model to accurately represent the outer mode is in line with the peak of tropical convective activity in parametrized models coinciding with the solar zenith (e.g. Rio *et al.*, 2009), and there is no reason that we should necessarily expect this common issue with global models to be magically fixed by the presence of a nearby MD.

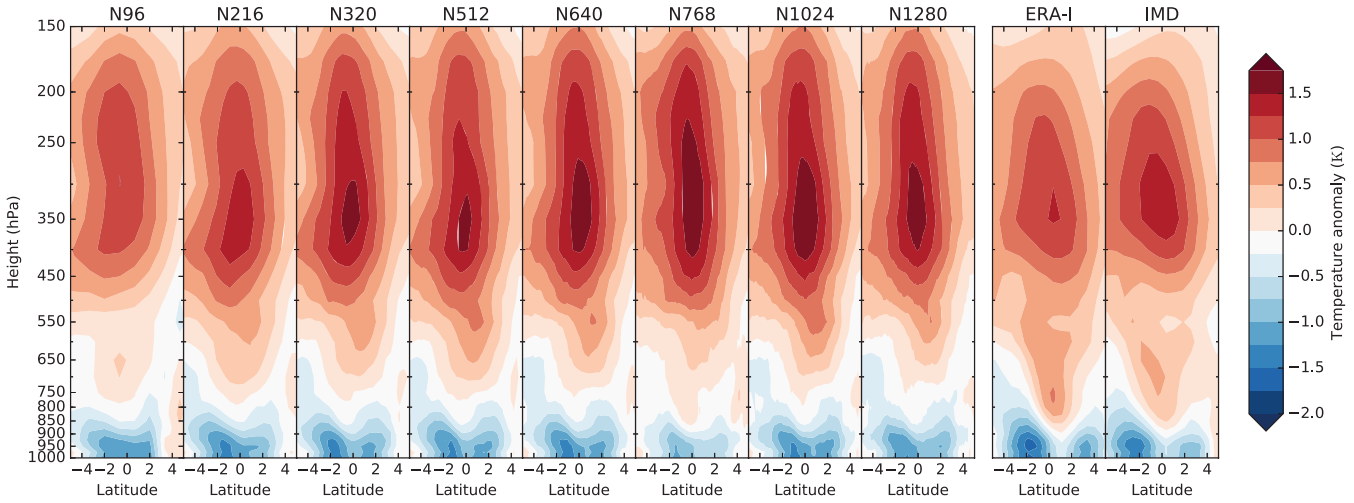

Figure 13. Mean composite temperature anomaly (K) for the case-study MDs. The compositing method is as in Figure 11. Here the anomaly is against the climatology computed for the 37 total forecast days (with these dates also used to compute climatology for the reanalysis structures.

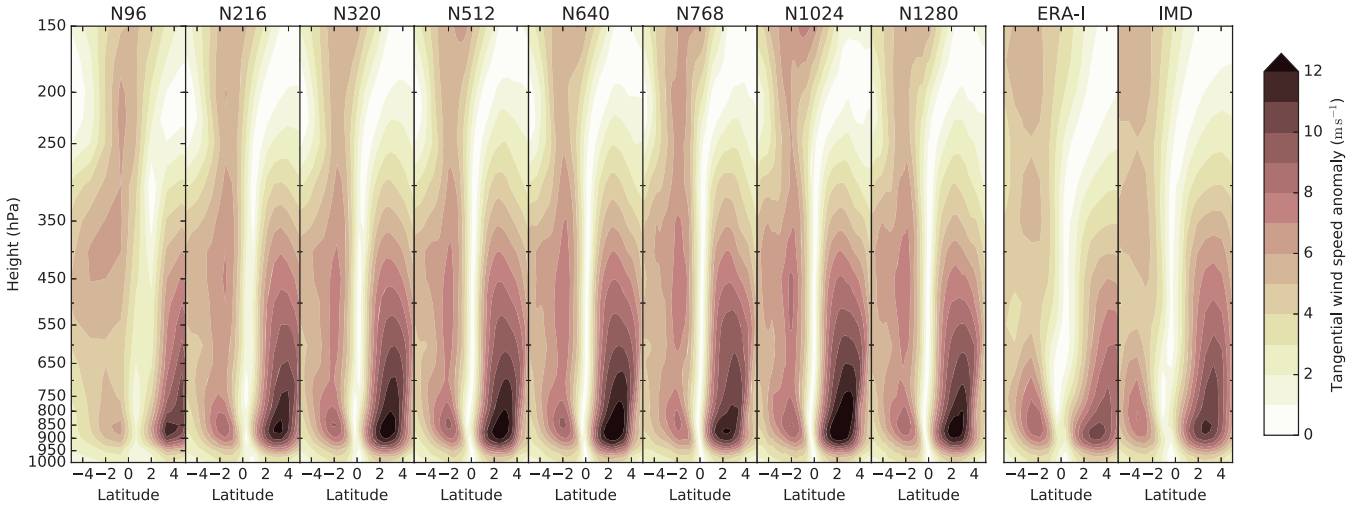

Figure 14. Mean composite wind speed anomaly ($\mathrm{m\,s^{-1}}$) for the case-study MDs. Construction of the composite is as Figure 11 and the anomaly is taken against the climatology, whose computation is as in Figure 13.

We next turn our focus to the representation of the central mode. This is responsible for 67% of the MD precipitation in observations (up to around 85% in the higher-resolution models), and MDs are in turn responsible for a majority of monsoon precipitation in northern India (Mooley, 1973), so it is clearly important that this is well represented in forecast models.

Figure 18 shows the values of A_{central} ($\mathrm{mm\,h^{-1}}$) as a function of time across all resolutions and for the climatology; as we might have expected from Table 3, resolutions greater than N512 capture the cycle very well with slight overestimation of the magnitude that is recovered slightly at N1280, although there is also a faint semidiurnal signal in the observations that does not

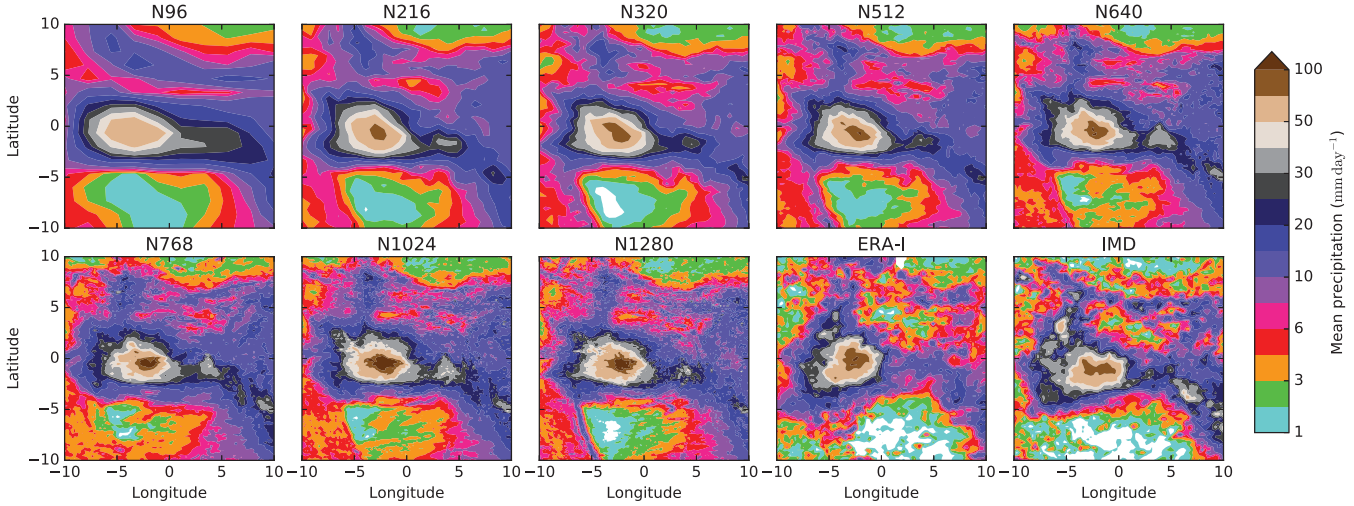

Figure 15. Composite total surface precipitation ($\mathrm{mm\,day^{-1}}$, method as in Figure 11), for all resolutions, as well as for the ERA-I and IMD case-study tracks as computed from TRMM 3B42.

Table 3. Values (mm h^{-1}) and times (UTC) of the maxima and minima for the outer (o-) and central (c-) modes of MD precipitation diurnal variability (i.e. A_{outer} and $A_{central}$ respectively), computed from fitting Eq. (4) to the respective composites for each resolution.

Resolution	c-mode min (time) c-mode max (time)	o-mode min (time) o-mode max (time)
TRMM	17.48 (0900)	7.52 (0300)
3B42	34.09 (0000)	15.58 (1200)
N1280	16.87 (1200)	2.35 (1200)
	39.25 (0000)	6.80 (0600)
N1024	17.66 (0900)	2.48 (1200)
	40.91 (0000)	6.58 (0600)
N768	16.28 (0900)	2.42 (1200)
	36.03 (0000)	6.56 (0600)
N640	15.81 (0900)	2.28 (1200)
	31.23 (0000)	6.54 (0600)
N512	13.87 (1200)	2.66 (1500)
	32.63 (0000)	6.29 (0600)
N320	12.43 (0900)	2.65 (1500)
	27.51 (0000)	6.18 (0600)
N216	13.38 (1200)	2.53 (1200)
	25.18 (0000)	6.39 (0000)
N96	5.32 (1500)	2.18 (1800)
	13.08 (0000)	5.36 (0000)

Also provided are the climatological values for MDs between 1998 and 2014 using TRMM 3B42 data, from Hunt *et al.* (2016b).

appear to be replicated by the model. This high fidelity at the finer resolutions is a strong indicator that the bulk of MD precipitation is not being generated by the convective parametrization scheme. We test this by interrogating the model output to determine whether this is the case, since the convective and microphysical (large-scale) schemes in the MetUM keep their precipitation output separate, so we can compute the composite ratio of stratiform/convective precipitation. Figure 19 shows the ratio of stratiform precipitation to total precipitation for the composite MD across all resolutions. We do not provide climatological values for comparison here, but the reader is encouraged to visit Figures 9 and 10 of Hunt *et al.* (2016b) and the associated discussion for the climatology as determined by TRMM's precipitation radar. As noted there, satellite observations regarding the attempted separation of precipitation into purely stratiform or convective mechanisms is non-trivial and is riddled with caveats. However, they produced climatologies at two different confidence levels: one where TRMM was essentially certain of the diagnosis either way (this left approximately half of the precipitation unaccounted for), and one where all precipitation was prescribed to either convective or stratiform regimes regardless of the certainty. It was speculated there, based on the work of Houze (1997), that for the latter case the stratiform fraction could be substantially overestimated and so we might expect Figure 19 to more closely resemble the 'definitely stratiform' regime presented by Hunt *et al.* (2016b). This is indeed the case, and therefore indicates one of two things: either the MetUM is underestimating stratiform precipitation in the monsoon trough region or TRMM precipitation radar is overestimating it. Based on our earlier analysis of the outer

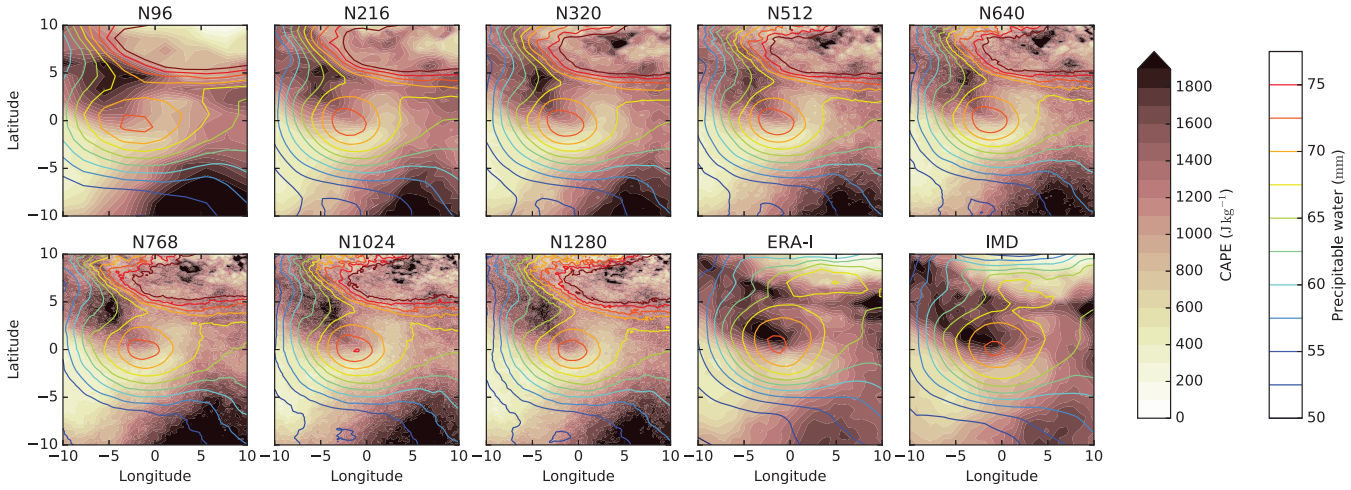

Figure 16. Composite CAPE (shading, J kg^{-1}) and total column precipitable water (line contours, mm) for each resolution, as well as for the ERA-I and IMD case-study tracks as computed from ERA-Interim.

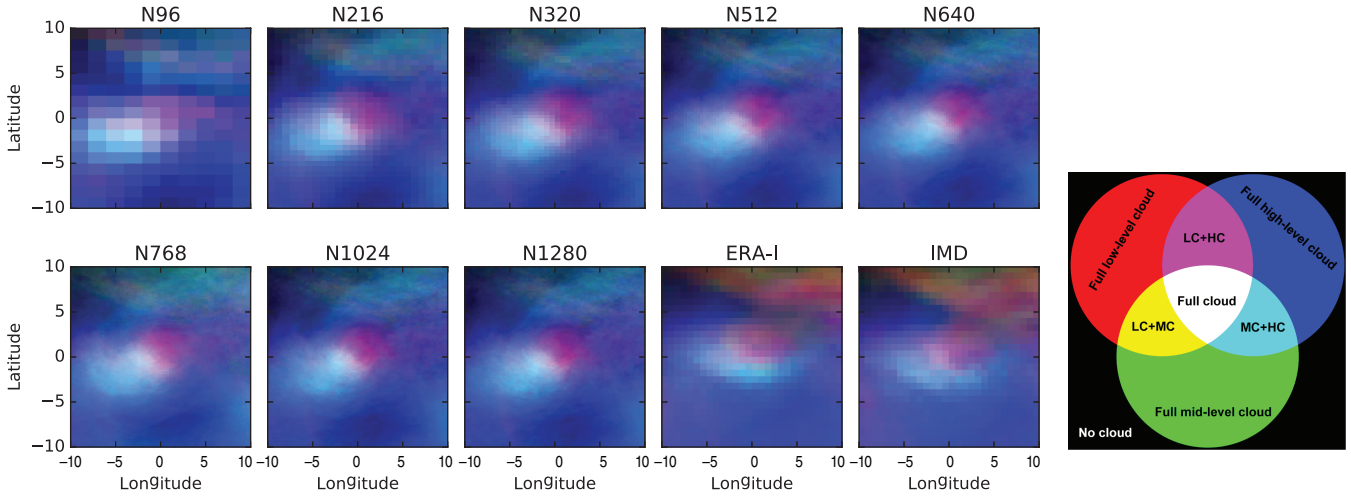

Figure 17. Composite cloud cover fraction for all resolutions, and ERA-I and IMD tracks determined from ERA-I. The bounding heights for the model cloud levels and for ERA-I reanalysis are given in section 5.3. The colour scheme is explained in the right-hand panel.

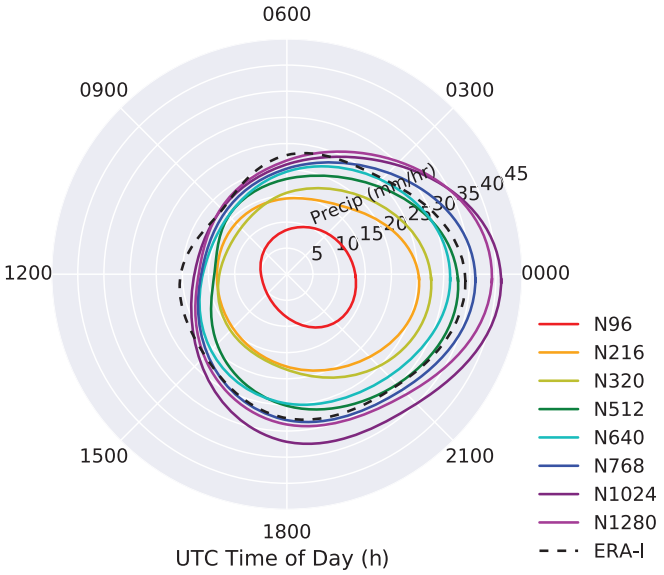

Figure 18. Amplitude, as a function of time (UTC) of the central (c-) mode for precipitation (mm h^{-1}) for MDs across all resolutions (solid coloured contours), and the climatology for ERA-I-tracked MDs in TRMM 3B42 (dashed black contour).

diurnal mode of precipitation and recent discussion, it seems most likely that the latter is true. Intercomparison of the ratios reveals that the increase in composite precipitation rate near the MD centre with finer model resolution is strongly correlated with increased stratiform precipitation, and representation over orography (Western Ghats, Himalayan foothills) is also improved.

6. Conclusions

We have examined the relationship between Indian monsoon depressions and horizontal resolution in the Met Office Unified Model. Seven case-studies were used in the global model at eight resolutions ranging from N96 (208 km) to N1280 (16 km). We then compared the resulting tracks, vertical and horizontal structure of the MDs, and the representation of the monsoon trough.

On the whole, we have seen that the MetUM represents the spatial structure of monsoon depressions fairly well. This improves with increasing resolution, but typically saturates at (i.e. there are diminishing returns beyond) N320 or N512 (well below the operational resolution of the Met Office, N768). Unfortunately, even at the lowest resolutions, the intensity across many fields is overestimated, a problem that increases with resolution but typically saturates at N320. That having been said, we have compared these fields to those in ERA-Interim, whose resolution falls between N216 and N320; without observations or reanalysis at a higher resolution, it is not possible to say with certainty that errors worsen in those fields compared to ERA-I. Even so, the mean rainfall structure and rate is generally well captured, including some finer detail, at N640 and above; and the same holds even for CAPE at N768 and above, although the structure is not as centralized as reanalysis suggests.

It is not clear why N320 is the resolution beyond which little improvement in representation is gained. One might suppose that among the phenomena important for the growth and sustainment of MDs, there are none with length-scale 15–60 km. This is plausible if we consider common mesoscale events in the subcontinent: mesoscale convective systems (MCSs) have a scale of the order of 10^5 m and are known to interact constructively with tropical depressions (e.g. Houze, 1989) whereas individual thunderstorms and convective cells have a length-scale of the order 10^3 m and are thus parametrized at all resolutions presented here. A detailed analysis, which has not been done here, would be needed to verify this.

We also looked at the diurnal cycle, finding that the mode governing the heavy (and typically mostly stratiform) rainfall associated with the central southwest maximum was well represented and had amplitude increasing with resolution with the optimal resolution being between N640 and N768. Conversely the mode associated with the weaker, larger-scale (mostly convective) precipitation is represented very poorly, a fact that does not change with resolution. This is likely due to the requirement of convective parametrization, a constraint that cannot be lifted until resolution reaches the order of 4 km (∼N5000). It remains an open question how models at convection-permitting resolution represent MDs and will be the subject of future work.

Overall, and taking into account the inflated cost of running higher-resolution models, it seems that a resolution of N512 (or at a push, N320) is sufficient to describe the composite MD structure in an initialised NWP model framework, although if one weights the track forecast highly, increasing this to N768 is recommended.

It is not clear what process in the model drives its tendency to overpredict MD intensity (although we again recall the caveat of low ERA-I resolution). We have seen that the mid-tropospheric warm anomaly is too strong, indicating too much latent heat

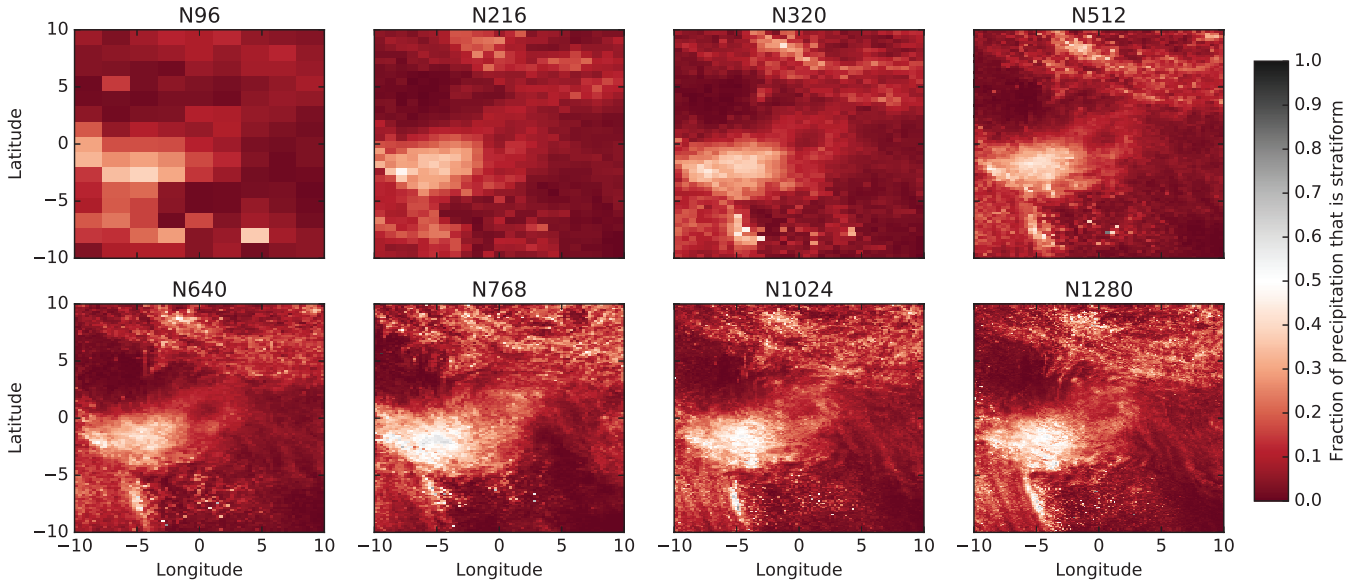

Figure 19. Composite fraction of surface precipitation caused by stratiform (as opposed to convective) processes in the model, across all resolutions. This is intended to allow direct comparison with the values from TRMM climatologies in Figures 9 and 10 of Hunt *et al.* (2016b).

release there, although this is not backed up by the presence of more mid-level cloud as one would expect. It is possible that the known difficulty of writing an effectual convective parametrization and the high dependence of tropical depressions on this convection is the prominent source of this bias, but correctly determining this would require a subsequent study to explore the sensitivity of MDs to model physics.

We have covered a range of resolutions also used in climate models (usually N512 and below). Although this problem differs slightly in that the MDs are not initialized, we can assume some similarity in structure is likely given the spin-up time in our case-studies. Based on the behaviour of the depression-trough, it seems likely that increasing resolution would cause a higher MD genesis rate, particularly in the north of the Bay of Bengal, where the trough deepens the most. This agrees in principle with the sensitivity tests of Johnson *et al.* (2016). Given the discussion above, we suspect that gains in structural representation would be marginal beyond N320.

Acknowledgements

(i) KMRH received partial support from the Met Office under the aegis of the NERC CASE studentship scheme, and was also supported by the NERC grant NE/L501608/1.
(ii) KMRH wishes to thank Paul Earnshaw and David Walters at the Met Office for their assistance with setting up the MetUM.
(iii) The authors wish to thanks three anonymous reviewers whose comments served to improve the clarity and coherence of this manuscript.
(iv) Andy Turner was supported by the INCOMPASS project (NERC grant number NE/L01386X/1).

Appendix

Formal description of system composite

The four-dimensional (three spatial axes, one temporal axis) composites for a given field are created by using the tracking data to find the centre of the MD at each time step in the output data (should one exist), and then extracting the surrounding data; that is to say, if all output data are precisely described by some function $f(x, y, z, t)$ and the disjoint[‖] sets of track loci are $\{x_n, y_n, t_n\}_m$, where m is the track index and n is the point index, and we specify some domain of interest, of side length L, invoking the notation $\Delta_i^x = (x_i - L, x_i + L)$ for the interval describing the domain centred on x_i, then the composite is simply the discontinuous function $f(\Delta^x_{n,m}, \Delta^y_{n,m}, z, t_{n,m})$. This function is just a finite-domain translation of the original, and the new horizontal axes are selected at each m, n such that $x_{m,n} = y_{m,n} = 0$, i.e. $f(\Delta^x_{n,m}, \Delta^y_{n,m}, z, t_{n,m}) \equiv g(x', y', z, t')$, where $x' = x - x_{n,m}$, $y' = x - y_{n,m}$, $t' = t_{n,m}$ and $f : \Delta^{x'}, \Delta^{y'}$. Thus to examine a mean vertical cross-section taken north to south, we compute $\overline{g(0, y', z, t')}$, where the bar denotes a time mean; for a mean horizontal composite at height Z, we would compute $\overline{g(x', y', Z, t')}$.

References

Abel SJ, Boutle IA. 2012. An improved representation of the raindrop size distribution for single-moment microphysics schemes. *Q. J. R. Meteorol. Soc.* **138**: 2151–2162. https://doi.org/10.1002/qj.1949.

Abel SJ, Shipway BJ. 2007. A comparison of cloud-resolving model simulations of trade wind cumulus with aircraft observations taken during RICO. *Q. J. R. Meteorol. Soc.* **133**: 781–794. https://doi.org/10.1002/qj.55.

Abel SJ, Walters DN, Allen G. 2010. Evaluation of stratocumulus cloud prediction in the Met Office forecast model during VOCALS-REx. *Atmos. Chem. Phys.* **10**: 10 541–10 559. https://doi.org/10.5194/acp-10-10541-2010.

Boville BA. 1991. Sensitivity of simulated climate to model resolution. *J. Clim.* **4**: 469–485. https://doi.org/10.1175/1520-0442(1991)004<0469:SOSCTM>2.0.CO;2.

Brown AR, Beare RJ, Edwards JM, Lock AP, Keogh SJ, Milton SF, Walters DN. 2008. Upgrades to the boundary-layer scheme in the Met Office numerical weather prediction model. *Boundary-Layer Meteorol.* **128**: 117–132. https://doi.org/10.1007/s10546-008-9275-0.

Bryan GH, Morrison H. 2012. Sensitivity of a simulated squall line to horizontal resolution and parameterization of microphysics. *Mon. Weather Rev.* **140**: 202–225. https://doi.org/10.1175/MWR-D-11-00046.1.

Buizza R, Petroliagis T, Palmer TN, Barkmeijer J, Hamrud M, Hollingsworth A, Simmons A, Wedi N. 1998. Impact of model resolution and ensemble size on the performance of an ensemble prediction system. *Q. J. R. Meteorol. Soc.* **124**: 1935–1960. https://doi.org/10.1002/qj.49712455008.

Catto JL, Shaffrey LC, Hodges KI. 2010. Can climate models capture the structure of extratropical cyclones? *J. Clim.* **23**: 1621–1635. https://doi.org/10.1175/2009JCLI3318.1.

Charney JG, Eliassen A. 1964. On the growth of the hurricane depression. *J. Atmos. Sci.* **21**: 68–75. https://doi.org/10.1175/1520-0469(1964)021<0068:OTGOTH>2.0.CO;2.

Chen TC, Yoon JH, Wang SY. 2005. Westward propagation of the Indian monsoon depression. *Tellus* **57A**: 758–769. https://doi.org/10.1111/j.1600-0870.2005.00140.x.

Dai A. 2006. Precipitation characteristics in eighteen coupled climate models. *J. Clim.* **19**: 4605–4630. https://doi.org/10.1175/JCLI3884.1.

Dee DP, Uppala SM, Simmons AJ, Berrisford P, Poli P, Kobayashi S, Andrae U, Balmaseda MA, Balsamo G, Bauer P, Bechtold P, Beljaars ACM, van de Berg L, Bidlot J, Bormann N, Delsol C, Dragani R, Fuentes M, Geer AJ, Haimberger L, Healy SB, Hersbach H, Hólm EV, Isaksen L, Kållberg P, Köhler M, Matricardi M, McNally AP, Monge-Sanz BM, Morcrette J-J, Park BK, Peubey C, de Rosnay P, Tavolato C, Thépaut J-N, Vitart F. 2011. The ERA-Interim reanalysis: Configuration and performance of the data assimilation system. *Q. J. R. Meteorol. Soc.* **137**: 553–597. https://doi.org/10.1002/qj.828.

Ditchek SD, Boos WR, Camargo SJ, Tippett MK. 2016. A genesis index for monsoon disturbances. *J. Clim.* **29**: 5189–5203. https://doi.org/10.1175/JCLI-D-15-0704.1.

Fritsch JM, Chappell CF. 1980. Numerical prediction of convectively driven mesoscale pressure systems. Part II: Mesoscale model. *J. Atmos. Sci.* **37**: 1734–1762. https://doi.org/10.1175/1520-0469(1980)037<1734:NPOCDM>2.0.CO;2.

Gentry MS, Lackmann GM. 2010. Sensitivity of simulated tropical cyclone structure and intensity to horizontal resolution. *Mon. Weather Rev.* **138**: 688–704. https://doi.org/10.1175/2009MWR2976.1.

Giorgi F, Marinucci MR. 1996. A investigation of the sensitivity of simulated precipitation to model resolution and its implications for climate studies. *Mon. Weather Rev.* **124**: 148–166. https://doi.org/10.1175/1520-0493(1996)124<0148:AIOTSO>2.0.CO;2.

Godbole RV. 1977. The composite structure of the monsoon depression. *Tellus* **29**: 25–40. https://doi.org/10.1111/j.2153-3490.1977.tb00706.x.

Grant ALM. 2001. Cloud-base fluxes in the cumulus-capped boundary layer. *Q. J. R. Meteorol. Soc.* **127**: 407–421. https://doi.org/10.1002/qj.49712757209.

Grant ALM, Brown AR. 1999. A similarity hypothesis for shallow-cumulus transports. *Q. J. R. Meteorol. Soc.* **125**: 1913–1936. https://doi.org/10.1002/qj.49712555802.

Gregory D, Allen S. 1991. 'The effect of convective scale downdrafts upon NWP and climate simulations'. In *Preprints, 9th Conference on Numerical Weather Prediction. Denver, CO*. American Meteorological Society: Boston, MA, pp. 122–123.

Gregory D, Rowntree PR. 1990. A mass flux convection scheme with representation of cloud ensemble characteristics and stability-dependent closure. *Mon. Weather Rev.* **118**: 1483–1506. https://doi.org/10.1175/1520-0493(1990)118<1483:AMFCSW>2.0.CO;2.

Gregory D, Kershaw R, Inness PM. 1997. Parametrization of momentum transport by convection. II: Tests in single-column and general circulation models. *Q. J. R. Meteorol. Soc.* **123**: 1153–1183. https://doi.org/10.1002/qj.49712354103.

Hill KA, Lackmann GM. 2009. Analysis of idealized tropical cyclone simulations using the Weather Research and Forecasting model: Sensitivity to turbulence parameterization and grid spacing. *Mon. Weather Rev.* **137**: 745–765. https://doi.org/10.1175/2008MWR2220.1.

Houze RA. 1989. Observed structure of mesoscale convective systems and implications for large-scale heating. *Q. J. R. Meteorol. Soc.* **115**: 425–461. https://doi.org/ 10.1002/qj.49711548702.

Houze RA. 1997. Stratiform precipitation in regions of convection: A meteorological paradox? *Bull. Am. Meteorol. Soc.* **78**: 2179–2196. https://doi.org/ 10.1175/1520-0477(1997)078<2179:SPIROC>2.0.CO;2.

Huffman GJ, Bolvin DT, Nelkin EJ, Wolff DB, Adler RF, Gu G, Hong Y, Bowman KP, Stocker EF. 2007. The TRMM multisatellite precipitation analysis (TMPA): Quasi-global, multiyear, combined-sensor precipitation estimates at fine scales. *J. Hydrometeorol.* **8**: 38–55. https://doi.org/ 10.1175/JHM560.1.

[‖] Of course, there is no mathematical reason that the sets of loci must be disjoint but, as yet, no two MDs have been observed to merge.

Hunt KMR, Parker DJ. 2016. The movement of Indian monsoon depressions by interaction with image vortices near the Himalayan wall. *Q. J. R. Meteorol. Soc.* **142**: 2224–2229. https://doi.org/ 10.1002/qj.2812.

Hunt KMR, Turner AG. 2016. The effect of soil moisture perturbations on Indian monsoon depressions in a numerical weather prediction model. *J. Clim*.

Hunt KMR, Turner AG, Inness PM, Parker DE, Levine RC. 2016a. On the structure and dynamics of Indian monsoon depressions. *Mon. Weather Rev.* **144**: 3391–3416. https://doi.org/ 10.1175/MWR-D-15-0138.1.

Hunt KMR, Turner AG, Parker DE. 2016b. The spatiotemporal structure of precipitation in Indian monsoon depressions. *Q. J. R. Meteorol. Soc.* **142**: 3195–3210. https://doi.org/ 10.1002/qj.2901.

Hurley JV, Boos WR. 2015. A global climatology of monsoon low pressure systems. *Q. J. R. Meteorol. Soc.* **141**: 1049–1064. https://doi.org/ 10.1002/qj.2447.

Johnson SJ, Levine RC, Turner AG, Martin GM, Woolnough SJ, Schiemann R, Mizielinski MS, Roberts MJ, Vidale PL, Demory ME Strachan J. 2016. The resolution sensitivity of the South Asian monsoon and Indo-Pacific in a global 0.35° AGCM. *Clim. Dyn.* **46**: 807–831. https://doi.org/ 10.1007/s00382-015-2614-1.

Keshavamurty RN, Asnani GC, Pillai PV, Das SK. 1978. Some studies of the growth of monsoon disturbances. *Proc. Indian Acad. Sci.-Sect. A: Earth Planet. Sci.* **87**: 61–75.

Krishnamurti TN, Kanamitsu M, Godbole RV, Chang CB, Carr F, Chow JH. 1975. Study of a monsoon depression (I). *J. Meteorol. Soc. Jpn.* **53**: 227–240.

Lock AP. 2001. The numerical representation of entrainment in parameterizations of boundary-layer turbulent mixing. *Mon. Weather Rev.* **129**: 1148–1163. https://doi.org/10.1175/1520-0493(2001)129<1148:TNROEI>2.0.CO;2.

Lock AP, Brown AR, Bush MR, Martin GM, Smith RNB. 2000. A new boundary-layer mixing scheme. Part I: Scheme description and single-column model tests. *Mon. Weather Rev.* **128**: 3187–3199. https://doi.org/ 10.1175/1520-0493(2000)128<3187:ANBLMS>2.0.CO;2.

Lott F, Miller MJ. 1997. A new subgrid-scale orographic drag parametrization: Its formulation and testing. *Q. J. R. Meteorol. Soc.* **123**: 101–127. https://doi.org/ 10.1002/qj.49712353704.

Martin GM, Ringer MA, Pope VD, Jones A, Dearden C, Hinton TJ. 2006. The physical properties of the atmosphere in the new Hadley Centre Global Environmental Model (HadGEM1). Part I: Model description and global climatology. *J. Clim.* **19**: 1274–1301. https://doi.org/ 10.1175/JCLI3636.1.

Mass CF, Ovens D, Westrick K, Colle BA. 2002. Does increasing horizontal resolution produce more skillful forecasts? *Bull. Am. Meteorol. Soc.* **83**: 407–430. https://doi.org/ 10.1175/1520-0477(2002)083<0407:DIHRPM>2.3.CO;2.

Mooley DA. 1973. Some aspects of Indian monsoon depressions and the associated rainfall. *Mon. Weather Rev.* **101**: 271–280. https://doi.org/ 10.1175/1520-0493(1973)101<0271:SAOIMD>2.3.CO;2.

Murakami H, Sugi M. 2010. Effect of model resolution on tropical cyclone climate projections. *SOLA* **6**: 73–76. https://doi.org/ 10.2151/sola.2010-019.

Pope V, Stratton R. 2002. The processes governing horizontal resolution sensitivity in a climate model. *Clim. Dyn.* **19**: 211–236. https://doi.org/ 10.1007/s00382-001-0222-8.

Prasad K, Kalsi SR, Datta RK. 1990. On some aspects of wind and cloud structure of monsoon depressions. *Mausam* **41**: 365–370.

Rio C, Hourdin F, Grandpeix J-Y, Lafore J-P. 2009. Shifting the diurnal cycle of parameterized deep convection over land. *Geophys. Res. Lett.* **36**: L07809. https://doi.org/ 10.1029/2008GL036779.

Roberts MJ, Vidale PL, Mizielinski MS, Demory ME, Schiemann R, Strachan J, Hodges K, Bell R, Camp J. 2015. Tropical cyclones in the UPSCALE ensemble of high-resolution global climate models. *J. Clim.* **28**: 574–596. https://doi.org/ 10.1175/JCLI-D-14-00131.1.

Roeckner E, Brokopf R, Esch M, Giorgetta M, Hagemann S, Kornblueh L, Manzini E, Schlese U, Schulzweida U. 2006. Sensitivity of simulated climate to horizontal and vertical resolution in the ECHAM5 atmosphere model. *J. Clim.* **19**: 3771–3791. https://doi.org/ 10.1175/JCLI3824.1.

Sarker RP, Choudhary A. 1988. A diagnostic study of monsoon depressions. *Mausam* **39**: 9–18.

Shukla J. 1978. CISK-barotropic-baroclinic instability and the growth of monsoon depressions. *J. Atmos. Sci.* **35**: 495–508. https://doi.org/ 10.1175/1520-0469(1978)035<0495:CBBIAT>2.0.CO;2.

Sikka DR. 1977. Some aspects of the life history, structure and movement of monsoon depressions. *Pure Appl. Geophys.* **115**: 1501–1529. https://doi.org/ 10.1007/BF00874421.

Sperber KR, Hameed S, Potter GL, Boyle JS. 1994. Simulation of the northern summer monsoon in the ECMWF model: Sensitivity to horizontal resolution. *Mon. Weather Rev.* **122**: 2461–2481. https://doi.org/ 10.1175/1520-0493(1994)122<2461:SOTNSM>2.0.CO;2.

Stano G, Krishnamurti TN, Vijaya Kumar TSV, Chakraborty A. 2002. Hydrometeor structure of a composite monsoon depression using the TRMM radar. *Tellus A* **54**: 370–381. https://doi.org/ 10.1034/j.1600-0870.2002.01330.x.

Stephens GL, L'Ecuyer T, Forbes R, Gettelmen A, Golaz J-C, Bodas-Salcedo A, Suzuki K, Gabriel P, Haynes J. 2010. Dreary state of precipitation in global models. *J. Geophys. Res. Atmos.* **115**: D24211. https://doi.org/ 10.1029/2010JD014532.

Strachan J, Vidale PL, Hodges K, Roberts M, Demory ME. 2013. Investigating global tropical cyclone activity with a hierarchy of AGCMs: The role of model resolution. *J. Clim.* **26**: 133–152. https://doi.org/ 10.1175/JCLI-D-12-00012.1.

Stratton RA, Stirling A, Derbyshire S. 2009. 'Changes and developments to convective momentum transport (CMT) parametrization based on analysis of CRM and SCM', Technical report 530. Met Office: Exeter, UK.

Tripoli GJ, Cotton WR. 1980. A numerical investigation of several factors contributing to the observed variable intensity of deep convection over south Florida. *J. Appl. Meteorol.* **19**: 1037–1063. https://doi.org/ 10.1175/1520-0450(1980)019<1037:ANIOSF>2.0.CO;2.

Walters DN, Brooks M, Boutle I, Melvin T, Stratton R, Wells H, Williams K, Bushell A, Copsey D, Earnshaw P, Edwards J, Gross M, Hardiman S, Harris C, Heming J, Klingaman N, Levine R, Manners J, Martin G, Milton S, Mittermaier M, Morcretter C, Riddick T, Roberts M, Sanchez C, Selwood P, Smith C, Tennant W, Vosper S, Vidale PL, Wilkinson J, Wood N, Woolnough S, Xavier P. 2016. The Met Office Unified Model Global Atmosphere 6.0/6.1 and JULES Global Land 6.0/6.1 configurations. *Geosci. Model Dev.* **10**(4): 1487–1520. https://doi.org/ 10.5194/gmd-2016-194.

Wilson DR, Ballard SP. 1999. A microphysically based precipitation scheme for the UK Meteorological Office Unified Model. *Q. J. R. Meteorol. Soc.* **125**: 1607–1636. https://doi.org/ 10.1002/qj.49712555707.

Wilson DR, Bushell AC, Kerr-Munslow AM, Price JD, Morcrette CJ. 2008. PC2: A prognostic cloud fraction and condensation scehem. I: Scheme description. *Q. J. R. Meteorol. Soc.* **134**: 2093–2107. https://doi.org/ 10.1002/qj.333.

Wood N, Mason PJ. 1993. The pressure force induced by neutral, turbulent flow over hills. *Q. J. R. Meteorol. Soc.* **119**: 1233–1267. https://doi.org/ 10.1002/qj.49711951402.

Wood N, Staniforth A, White AA, Allen T, Diamantakis M, Gross M, Melvin T, Smith C, Vosper S, Zerroukat M, Thuburn J. 2014. An inherently mass-conserving semi-implicit semi-Lagrangian discretization of the deep-atmosphere global non-hydrostatic equations. *Q. J. R. Meteorol. Soc.* **140**: 1505–1520. https://doi.org/ 10.1002/qj.2235.